

The physics of angular momentum radio

B. Thidé,^{1,*} F. Tamburini,^{2,†} H. Then,³ C. G. Smeda,² and R. A. Ravanelli⁴

¹Swedish Institute of Space Physics, Ångström Laboratory, P. O. Box 537, SE-75121 Uppsala, Sweden, EU

²Twist Off S.R.L., via della Croce Rossa 112, IT-35129 Padova, Italy, EU

³University of Bristol, Department of Mathematics, University Walk, Bristol BS8 1TW, England, UK

⁴SIAE Microelettronica, 21, via Michelangelo Buonarroti, IT-20093 Cologno Monzese, Milan, Italy, EU

(Dated: 2014-10-16 02:19:10 +0200 (Thu, 16 Oct 2014))

Wireless communications, radio astronomy and other radio science applications are mainly implemented with techniques built on top of the electromagnetic linear momentum (Poynting vector) physical layer. As a supplement and/or alternative to this conventional approach, techniques rooted in the electromagnetic angular momentum physical layer have been advocated, and promising results from proof-of-concept radio communication experiments using angular momentum were recently published. This sparingly exploited physical observable describes the rotational (spinning and orbiting) physical properties of the electromagnetic fields and the rotational dynamics of the pertinent charge and current densities. In order to facilitate the exploitation of angular momentum techniques in real-world implementations, we present a systematic, comprehensive theoretical review of the fundamental physical properties of electromagnetic angular momentum observable. Starting from an overview that puts it into its physical context among the other Poincaré invariants of the electromagnetic field, we describe the multi-mode quantized character and other physical properties that sets electromagnetic angular momentum apart from the electromagnetic linear momentum. These properties allow, among other things, a more flexible and efficient utilization of the radio frequency spectrum. Implementation aspects are discussed and illustrated by examples based on analytic and numerical solutions.

PACS numbers: 03.65.Ud,14.70.Bh,42.50.Tx

I. INTRODUCTION

Transferring information wirelessly by means of electromagnetic fields amounts to encoding information onto physical observables carried by these fields, radiating the observables as local volumetric densities into the surrounding space, and converting these densities remotely into observables using integrating sensors connected to information-decoding receivers. The volumetric density of each observable is second order in the fields, falls off asymptotically as the square of the distance from the source, and fulfills a conservation law. Of all physical observables carried by the electromagnetic field, only the linear momentum (volume integrated Poynting vector, “power”) is fully exploited in present-day radio science and applications related to wireless information transfer.

A fundamental physical limitation of the linear momentum observable, which describes the *translational* degrees of freedom of the electromagnetic field, is that it is single-mode in the sense that a linear momentum radio communication link comprising one single transmitting and one single receiving transducer of a conventional type (*e.g.*, a half-wave dipole antenna), known as a single-input-single-output (SISO) link, provides only one physical channel per carrier frequency.

In contrast, electromagnetic angular momentum, the physical observable that describes the *rotational* degrees of freedom

of the electromagnetic field, is multi-mode, being a superposition of discrete, classical electromagnetic angular momentum eigenmodes, each uniquely identified by the number of 2π that the phase varies azimuthally during one period, *i.e.*, by its topological charge. Hence, a wireless communication link where the transmitting and receiving ends each are equipped with a single, monolithic transducer allowing the charges to move in two and three dimensions so that it is able to generate and/or detect angular momentum modes directly, constitutes an angular momentum SISO link system. Such a system has the capability to accommodate multiple physical channels for information transfer on a single carrier frequency within the same frequency bandwidth as that of a single-channel linear momentum SISO system. The actual number of physical angular momentum channels that can be used in a certain application is limited classically only by engineering and implementation issues.

The multi-mode capability of systems based on electromagnetic angular momentum is a consequence of the fact that different eigenmodes are topologically distinct and linearly independent by virtue of their mutual functional orthogonality in a Hilbert space of denumerably infinite dimension. These mathematical properties ensure that the angular momentum eigenmodes are physically separable and therefore can accommodate multiple independent data streams even in situations when the modes occupy the same frequency and overlap each other in space and time.

In order to put angular momentum into its proper physical context and on a firm theoretical basis, we first review the properties of the electromagnetic field that makes wireless information transfer possible. Then we continue with a rather detailed theoretical presentation of the physics itself, touching upon first quantization quantum aspects of classical electrodynamics and its observables.

* Electronic address: bt@irfu.se; Home page: www.physics.irfu.se/~bt; Also at: University of Padua, Scuola Galileiana di Studi Superiori, via VIII Febbraio 1848 n. 2, IT-35122 Padua, Italy, EU.

† Electronic address: fabrizio.tamburini@unipd.it; Also at: University of Padua, Department of Physics and Astronomy, via Marzolo 8, IT-35131 Padua, Italy, EU.

Furthermore, concepts and issues related to the exploitation of the angular momentum physical layer and practical implementations are discussed in general terms both formally and by way of examples.

A theoretical description of electromagnetic angular momentum in the context of the ten Poincaré invariants and the associated conservation laws is presented in an Appendix. In another Appendix we derive exact expressions, valid in all space, for the fields from one or more electric Hertzian dipoles, as well as the second-order field quantities that enters the expressions for the linear and angular momentum densities carried by these fields.

II. BACKGROUND

The fundamental physical property of the classical electromagnetic field (\mathbf{E}, \mathbf{B}) that renders wireless information transfer possible is its capability to transport physical observables, *i.e.*, directly measurable intrinsic and extrinsic electromagnetic quantities, over long distances through free space, solids, fluids, gases, and plasma. The observables are generated within a volume of finite spatial extent (the source volume V'), and then propagated in the form of volumetric densities to a remotely located volume of likewise finite spatial extent (the observation volume V) where these densities are volume integrated into observables and the information carried by them subsequently decoded and analyzed. Each electromagnetic observable density is second order (quadratic or bilinear) in the fields \mathbf{E} and \mathbf{B} and fulfills an equation of continuity. In classical physics terms these observables can be viewed as the result of the changes in the dynamics, *e.g.*, acceleration, of the charged particles in the source volume and, causally, in the observation volume.

In classical electrodynamics the interplay between the microscopic electric charge and current densities $\rho^e(t, \mathbf{x})$ and $\mathbf{j}^e(t, \mathbf{x})$ and the electric and magnetic fields, $\mathbf{E}(t, \mathbf{x})$ and $\mathbf{B}(t, \mathbf{x})$, and between the fields themselves are described by the Maxwell-Lorentz equations. Allowing also for magnetic charge and current densities, represented by the pseudoscalar ρ^m and the pseudovector \mathbf{j}^m , respectively, [1–3], these equations can be extended to the more symmetrical form [4–6]

$$\nabla \cdot \mathbf{E} = \frac{\rho^e}{\epsilon_0} \quad (1a)$$

$$\nabla \cdot \mathbf{B} = \frac{\rho^m}{\epsilon_0 c^2} \quad (1b)$$

$$\nabla \times \mathbf{E} + \frac{\partial \mathbf{B}}{\partial t} = -\frac{1}{\epsilon_0 c^2} \mathbf{j}^m \quad (1c)$$

$$\nabla \times \mathbf{B} - \frac{1}{c^2} \frac{\partial \mathbf{E}}{\partial t} = \frac{1}{\epsilon_0 c^2} \mathbf{j}^e \quad (1d)$$

where c is the speed of light in free space and ϵ_0 is the dielectric permittivity of free space. This set of linear, inhomogeneous, coupled, partial differential equations are the postulates of classical electrodynamics from which all properties of the classical electromagnetic field, its observables, and interactions can be derived. These postulates are valid for radio and optical wavelengths alike inasmuch as they are scale invariant and are

Table I. Various second-order products of the Riemann-Silberstein vector $\mathbf{G} = \mathbf{E} + ic\mathbf{B}$ with itself and their meaning in terms of quadratic and bilinear products of the fields \mathbf{E} and \mathbf{B} . Complex conjugate is denoted by an asterisk (*).

Complex-valued notation	Real-valued notation
$\mathbf{G} \cdot \mathbf{G}$	$\mathbf{E} \cdot \mathbf{E} - c^2 \mathbf{B} \cdot \mathbf{B} + 2ic\mathbf{E} \cdot \mathbf{B}$
$\mathbf{G} \cdot \mathbf{G}^* = \sqrt{(\mathbf{G} \cdot \mathbf{G})(\mathbf{G} \cdot \mathbf{G})^*}$	$\mathbf{E} \cdot \mathbf{E} + c^2 \mathbf{B} \cdot \mathbf{B} \equiv E^2 + c^2 B^2$
$\mathbf{G} \times \mathbf{G}$	$\mathbf{0}$
$\mathbf{G} \times \mathbf{G}^* = -\mathbf{G}^* \times \mathbf{G}$	$-2ic(\mathbf{E} \times \mathbf{B})$
$\mathbf{G} \otimes \mathbf{G}$	$\mathbf{E} \otimes \mathbf{E} - c^2 \mathbf{B} \otimes \mathbf{B} + ic(\mathbf{E} \otimes \mathbf{B} + \mathbf{B} \otimes \mathbf{E})$
$\mathbf{G}^* \otimes \mathbf{G}^* = (\mathbf{G} \otimes \mathbf{G})^*$	$\mathbf{E} \otimes \mathbf{E} - c^2 \mathbf{B} \otimes \mathbf{B} - ic(\mathbf{E} \otimes \mathbf{B} + \mathbf{B} \otimes \mathbf{E})$
$\mathbf{G} \otimes \mathbf{G}^*$	$\mathbf{E} \otimes \mathbf{E} + c^2 \mathbf{B} \otimes \mathbf{B} - ic(\mathbf{E} \otimes \mathbf{B} - \mathbf{B} \otimes \mathbf{E})$
$\mathbf{G}^* \otimes \mathbf{G} = (\mathbf{G} \otimes \mathbf{G}^*)^*$	$\mathbf{E} \otimes \mathbf{E} + c^2 \mathbf{B} \otimes \mathbf{B} + ic(\mathbf{E} \otimes \mathbf{B} - \mathbf{B} \otimes \mathbf{E})$

therefore valid for classical wireless information transfer at all frequencies.

It is convenient to express the fields $\mathbf{E}, \mathbf{B} \in \mathbb{R}^3$ in terms of the complex-valued Riemann-Silberstein vector [7–11]

$$\mathbf{G}(t, \mathbf{x}) = \mathbf{E}(t, \mathbf{x}) + ic\mathbf{B}(t, \mathbf{x}) \in \mathbb{C}^3, \quad i^2 = -1 \quad (2)$$

some properties of which are listed in Table I, and to express the charge and current densities in the complex-valued forms

$$\rho(t, \mathbf{x}) = \rho^e(t, \mathbf{x}) + \frac{i}{c} \rho^m(t, \mathbf{x}) \quad (3a)$$

$$\mathbf{j}(t, \mathbf{x}) = \mathbf{j}^e(t, \mathbf{x}) + \frac{i}{c} \mathbf{j}^m(t, \mathbf{x}) \quad (3b)$$

Dirac's symmetrized Maxwell-Lorentz equations (1) then attain the complex-valued form

$$\nabla \cdot \mathbf{G} = \frac{\rho}{\epsilon_0} \quad (4a)$$

$$\nabla \times \mathbf{G} = \frac{i}{c} \frac{\partial \mathbf{G}}{\partial t} + \frac{i}{\epsilon_0 c} \mathbf{j} \quad (4b)$$

Following Białyński-Birula and Białyńska-Birula [12, 13], who instead of \mathbf{G} use a differently normalized complex vector, *viz.* $\mathbf{F} = \mathbf{G}\sqrt{\epsilon_0/2}$, we first introduce the linear momentum operator for the field,

$$\hat{\mathbf{p}}^{\text{field}} = \sum_{j=1}^3 \hat{\mathbf{x}}_j \hat{p}_j^{\text{field}} = \sum_{j=1}^3 \hat{\mathbf{x}}_j \left(-i\hbar \frac{\partial}{\partial x_j} \right) = -i\hbar \nabla \quad (5)$$

where \hbar is the normalized Planck constant. Secondly, we introduce the vector-like symbolic construct

$$\mathbf{S} \equiv \sum_{j=1}^3 S_j \hat{\mathbf{x}}_j \quad (6)$$

with components

$$S_1 = \begin{pmatrix} 0 & 0 & 0 \\ 0 & 0 & -i \\ 0 & i & 0 \end{pmatrix} \quad S_2 = \begin{pmatrix} 0 & 0 & i \\ 0 & 0 & 0 \\ -i & 0 & 0 \end{pmatrix} \quad S_3 = \begin{pmatrix} 0 & -i & 0 \\ i & 0 & 0 \\ 0 & 0 & 0 \end{pmatrix} \quad (7)$$

i.e., the spin-1 matrices fulfilling the angular momentum commutation rule

$$[S_i, S_j] = -i\epsilon_{ijk}S_k, \quad (8)$$

where

$$\epsilon_{ijk} = \begin{cases} 1 & \text{if } i, j, k \text{ is an even permutation of } 1, 2, 3 \\ 0 & \text{if at least two of } i, j, k \text{ are equal} \\ -1 & \text{if } i, j, k \text{ is an odd permutation of } 1, 2, 3 \end{cases} \quad (9)$$

is the fully antisymmetric rank-3 pseudotensor (the Levi-Civita symbol). Then, thirdly, we introduce the field helicity operator

$$\hat{\Lambda} = \frac{\mathbf{S} \cdot \hat{\mathbf{p}}^{\text{field}}}{|\hat{\mathbf{p}}^{\text{field}}|} \equiv \frac{\sum_{j=1}^3 S_j \hat{p}_j^{\text{field}}}{|\hat{\mathbf{p}}^{\text{field}}|} \quad (10)$$

This allows us to write the Maxwell-Lorentz equations (1) in free space and other domains where $\rho^e = \rho^m = 0$ and $\mathbf{j}^e = \mathbf{j}^m = \mathbf{0}$ in the form

$$\hat{\mathbf{p}}^{\text{field}} \cdot \mathbf{G} = 0 \quad (11a)$$

$$i\hbar \frac{\partial \mathbf{G}}{\partial t} = \hat{H}^{\text{field}} \mathbf{G} \quad (11b)$$

where

$$\hat{H}^{\text{field}} = c|\hat{\mathbf{p}}^{\text{field}}|\hat{\Lambda} = c\mathbf{S} \cdot \hat{\mathbf{p}}^{\text{field}} \equiv c \sum_{j=1}^3 S_j \hat{p}_j^{\text{field}} \quad (12)$$

Recalling the quantal relation $\hat{\mathbf{p}}^{\text{field}} = \hbar\mathbf{k}$, where \mathbf{k} is the wave vector, we see that the first equation, Eqn. (11a), is the transversality condition, $\mathbf{k} \perp \mathbf{G}$, for electromagnetic waves propagating in free space, whereas the second equation, Eqn. (11b), describes the dynamics of the field and takes the form of a Schrödinger/Pauli/Dirac equation where \hat{H}^{field} behaves as a Hamiltonian operator for the free electromagnetic field. The electromagnetic theory that corresponds to classical mechanics is the geometrical optics (eikonal, “ray optics”) approximation of the Maxwell-Lorentz equations [14].

The solutions of Eqn. (11b) can, in certain aspects, be viewed as first quantization photon wave functions that obey the superposition principle [3, 14–39]. However, Cohen-Tannoudji *et al.* [40, p. 204] argue against “... suggesting (in spite of warnings) the false idea that the Maxwell waves are the wave functions of the photon.”

Electromagnetic observables that can be physically measured directly and therefore be used in radio and optical science and technology applications are linear combinations of second order (quadratic, bilinear) quantities such as $\mathbf{E} \cdot \mathbf{E}$, $\mathbf{B} \cdot \mathbf{B}$, $\mathbf{E} \times \mathbf{B}$, $\mathbf{x} \times (\mathbf{E} \times \mathbf{B})$, and similar and can be accurately calculated from the first order fields \mathbf{E} and \mathbf{B} that are solutions of Eqns. (1).

In fact, as was pointed out by Silberstein [8, 9], it is very convenient to calculate these second order quantities in a formalism based on the complex vector representation given by Eqn. (2), today known as the Majorana-Oppenheimer formalism. This formalism is also convenient for canonical (second) quantization of the electromagnetic field [12, 30].

However, the fields themselves are abstractions in the sense that they cannot be measured directly but have to be estimated from measurements of physical observables that are quadratic or bilinear in the fields. To quote what Dyson [41] wrote in a very insightful and readable essay:

“Fields are an abstract concept, far removed from the familiar world of things and forces.”

“The modern view of the world that emerged from Maxwell’s theory is a world with two layers. The first layer, the layer of the fundamental constituents of the world, consists of fields satisfying simple linear equations. The second layer, the layer of the things that we can directly touch and measure, consists of mechanical stresses and energies and forces. The two layers are connected, because the quantities in the second layer are quadratic or bilinear combinations of the quantities in the first layer. . . . The objects on the first layer, the objects that are truly fundamental, are abstractions not directly accessible to our senses. The objects that we can feel and touch are on the second layer, and their behavior is only determined indirectly by the equations that operate on the first layer. The two-layer structure of the world implies that the basic processes of nature are hidden from our view.”

“... the objects that are truly fundamental, are abstractions not directly accessible to our senses. . . . It means that an electric field-strength is an abstract quantity, incommensurable with any quantities that we can measure directly.”

“It may be helpful for the understanding of quantum mechanics to stress the similarities between quantum mechanics and the Maxwell theory.”

Hence, in order to satisfactorily assess and optimally exploit the information-carrying capability of the electromagnetic field in all conceivable application scenarios in radio and optics, it is essential to analyze not only the properties of the fields as such but also the properties of the electromagnetic observables, which are second order in the fields. In Sect. III we will show that the physical observables themselves (the volume integrated densities) all tend to a constant value when they propagate in free space and the distance from the radiation source tends to infinity. This means that there exists no finite distance from the source beyond which any of these observables tends to zero or vanishes identically. Consequently, they can all carry information over arbitrary large distances in free space, albeit subject to engineering limitations (angular distribution, sensor area, detector sensitivity, noise, integration time, . . .).

However, of all physical observables that may potentially be used for wireless information transfer, present-day radio science and engineering implementations almost exclusively exploit only the linear momentum observable. This is because a conventional linear receiving antenna is an observation volume V in the form of a very thin cylinder where the charges are

constrained to move in one dimension in the form of a conduction current; this current is carried by the electrons that can be viewed as moving relative to a fixed neutralizing background without recoil. Such an antenna, typically with a length L of the order half a wavelength, senses a projection of the field linear momentum density vector and integrates the component of the electric conduction current density vector $\mathbf{j}^e(t, \mathbf{x})$ over L along the axis of the cylinder into a time-varying, spatially averaged scalar conduction current. This spatially averaged scalar current is fed to the receiver equipment (usually an electronics device) where it is processed and the wirelessly transferred information is extracted. In the process, the vector character of the current density is discarded and hence information is lost.

Linear momentum wireless information transfer techniques have the advantage that they are simple, robust, and easy to implement, but have the drawback that they can be wasteful when it comes to the use of the frequency spectrum. This is because electromagnetic linear momentum is single-mode, allowing only one independent linear-momentum physical channel of information transfer per carrier frequency (per wave polarization, per antenna). The ensuing over-crowding of the radio frequency bands, often referred to as the ‘‘spectrum crunch’’, has become a serious problem in radio communications and also imposes limitations on radio astronomy and other radio science applications as well as on fiber optics communications. It is doubtful whether further evolutionary refinements of conventional techniques and methods built on the linear momentum density (*i.e.*, Poynting vector) physics layer alone will, in the long term, suffice to remedy these problems.

This situation has led to the idea of exploiting so far underutilized physical observables of the electromagnetic field that do not suffer from the inherent information-carrying limitation of present-day radio techniques. The development and exploitation of a new physical layer that has a higher information-carrying capacity per unit bandwidth already at the fundamental physics level, before any multi-transducer or other spectral density enhancing techniques are applied at the engineering application layer, sets the stage for new radio paradigms that may enable a wiser exploitation of the radio frequency spectrum resource.

Specifically, it has been proposed that the electromagnetic angular momentum (moment of momentum), discussed already by Maxwell in his writings in the 1860’s [42], studied by other authors since over a century [43–46], and nowadays treated in standard physics textbooks [3, 4, 40, 47–55], be fully exploited in radio science and technology [5, 56–62]. The rationale being that it has been demonstrated in experiments at microwave and optical wavelengths that by exploiting the electromagnetic angular momentum, one can drastically increase the information-carrying capacity of wireless communications [63–67].

This increase is mainly due to the fact that angular momentum is discretized (quantized) already at the classical level. An arbitrary angular momentum state is namely a superposition of discrete classical angular momentum eigenmodes that are mutually orthogonal in a Hilbert space [56, 64, 68–73]. Each eigenmode is characterized by a unique integer that denotes its topological charge, corresponding to the azimuthal quantum

number (mode index).

As an illustration of how one can increase the information-carrying capacity of a radio beam by exploiting the fundamental physical properties of its angular momentum, let us consider a cylindrical symmetric beam where the individual electric field vectors $\mathbf{E}(t, \mathbf{x})$ (and the associated magnetic field vectors) are expressed in cylindrical coordinates (ρ, φ, z) as

$$\mathbf{E}(t, \mathbf{x}) = \mathbf{E}(t, \rho, \varphi, z) = \mathbf{E}_0 R(\rho) \Phi(\varphi) Z(z) T(t) e^{i(k_z z - \omega t)} \quad (13)$$

where \mathbf{E}_0 is a constant vector, R is the radial part, Φ is the azimuthal part, T is slowly varying as a function of time t , Z is slowly varying as a function of longitudinal distance z , and k_z is the z component of the wave vector, corresponding to the z (longitudinal) component the linear momentum $p_z = \hbar k_z$ of each photon of the field.

If $\Phi(\varphi)$ is well-behaved enough that it can be represented by a Fourier series

$$\Phi(\varphi) = \sum_{m=-\infty}^{\infty} c_m e^{im\varphi} \quad (14)$$

then, according to Eqn. (A53c), the z component of the orbital angular momentum (OAM) is

$$\begin{aligned} \hat{L}_z^{\text{field}} \mathbf{E}(t, \mathbf{x}) &= -i\hbar \frac{\partial}{\partial \varphi} \mathbf{E}(t, \mathbf{x}) \\ &= \sum_{m=-\infty}^{\infty} c_m m \hbar \mathbf{E}_0 R(\rho) Z(z) T(t) e^{i(m\varphi + k_z z - \omega t)} \end{aligned} \quad (15)$$

i.e., a weighted superposition of L_z^{field} eigenstates

$$\mathbf{E}_m(t, \mathbf{x}) = \mathbf{E}_0 R(\rho) Z(z) T(t) e^{i(m\varphi + k_z z - \omega t)} \quad (17)$$

In particular,

$$\hat{L}_z^{\text{field}} \mathbf{E}_m = m \hbar \mathbf{E}_m \quad (18)$$

which means that the z component of the orbital angular momentum of each photon in this beam is $m\hbar$.

The quantization of the orbital part of the classical electromagnetic angular momentum just demonstrated is a consequence of the single-valuedness of the electromagnetic fields upon their winding an integer number of 2π in azimuth angle φ around the beam axis z , resulting in a Bohr-Sommerfeld type quantization condition [49, 74–77]. It should be stressed that this quantum property exists already at the classical electrodynamics (Maxwell) level. Mathematically it can be expressed in terms of Hilbert space orthogonality between the OAM eigenstates $\langle m_1 |$ and $| m_2 \rangle$ as follows:

$$\begin{aligned} \langle m_1 | m_2 \rangle &= \int_V d^3x (\mathbf{E}_{m_1})^* \cdot \mathbf{E}_{m_2} \\ &= \mathbf{E}_0 Z(z) T(t) e^{i(k_z z - \omega t)} \int_{\rho_1}^{\rho_2} d\rho R(\rho) \int_0^{2\pi} d\varphi (e^{im_1\varphi})^* e^{im_2\varphi} \\ &= \text{Const} \times \mathbf{E}_0 Z(z) T(t) e^{-i(\omega t - k_z z)} \delta_{m_1 m_2} \end{aligned} \quad (19)$$

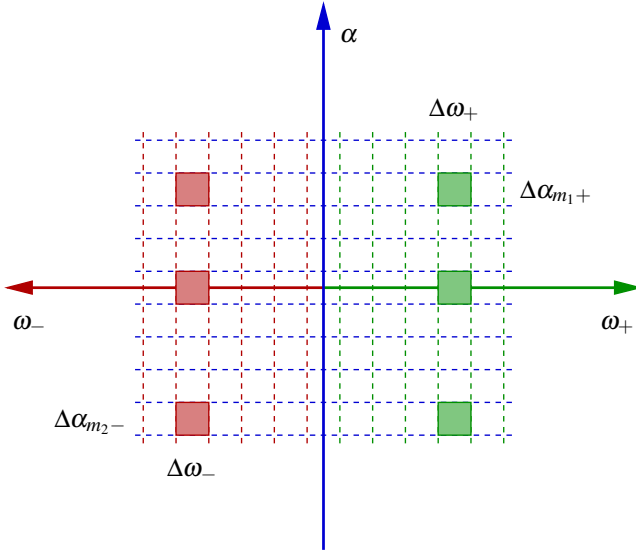


Figure 1. The two-dimensional oscillation/rotation plane spanned by the temporal phase oscillation rate, *i.e.*, the frequency ω (horizontal axis), and the angular phase rotation rate α , *i.e.*, the z component of the orbital angular momentum (OAM) L_z (vertical axis) in units of Planck's normalized constant \hbar . The right-hand, green part of the horizontal axis represents right-hand circular polarization (spin), and the left-hand, red part of the axis represents the opposite, right-hand circular polarization (spin). The α axis is rasterized into rotational frequency bins of azimuthal mode numbers m because of the single-valuedness of the fields that causes a quantization of L_z , and the ω axes are rasterized in terms of bandwidth segments. The solid green squares in the right-hand plane represent different transmission channels on the same carrier frequency ω_+ , with the same frequency bandwidth $\Delta\omega_+$, and in the same spin (polarization) state $\sigma = +1$, but in different rotational frequency bins α_{m_1} and α_{m_2} , corresponding to two different OAM azimuthal quantum numbers m_1 and m_2 , respectively. The solid red squares in the left-hand plane represent transmission channels with the same carrier frequency ($\omega_- = \omega_+$) and frequency bandwidth ($\Delta\omega_- = \Delta\omega_+$) as for the right-hand (green) plane, but in the opposite spin state $\sigma = -1$, allowing a more optimum use of the frequency spectrum. All possible squares in the (ω_{\pm}, α) plane constitute unique, independent information transfer eigenmode channels $(\omega, \sigma, \alpha_m)$. For instance, the six solid squares in the figure use the same carrier frequency and occupy the same frequency bandwidth. This is therefore an example of a six-fold frequency re-use.

where $\delta_{m_1 m_2}$ is the Kronecker delta. This orthogonality ensures that different L_z eigenmodes \mathbf{E}_m can co-exist on the same carrier frequency ω and in the same polarization state σ , allowing a simultaneous transfer of different information streams independently, without the need for extra frequency bandwidth.

In other words, OAM spans a state space of dimension $N = 1, 2, 3, \dots$, and can therefore be regarded as an ‘‘azimuthal (tangential) polarization’’ with arbitrarily many states [65]. This makes it possible, at least in principle, to use OAM to physically encode an unlimited amount of information onto any part of an EM beam, down to the individual photon [78, 79].

In the particular case that

$$\Phi(\varphi) = e^{ik_{\varphi}\rho\varphi} \equiv e^{i\alpha\varphi} \quad (20)$$

where k_{φ} is the φ (azimuthal) component of the wave vector, and α has a non-integer value, the Fourier amplitudes are [60, 68]

$$c_m = \frac{\exp(i\pi\alpha) \sin(\pi\alpha)}{\pi(\alpha - m)} \quad (21)$$

Hence, an electromagnetic beam carrying an arbitrary amount α of OAM is a superposition of discrete classical OAM eigenmodes \mathbf{E}_m [80] that are mutually orthogonal in a function space sense and therefore propagate independently of each other [81].

For a beam of electromagnetic waves that propagates along a given direction, chosen to be the z axis in a cylindrical coordinate system, the phase factor of the waves is typically $e^{i\beta}$ where $\beta = \alpha\varphi + k_z z - \omega t$. From Eqn. 20 we see that $\alpha = k_{\varphi}\rho$ where k_{φ} is the azimuthal wave number, and therefore the z component of the angular momentum in units of \hbar carried by the beam. This angular momentum adds, in effect, an extra dimension of periodic variation, augmenting the one-dimensional ordinary frequency axis to a two-dimensional frequency plane as outlined graphically in Fig. 1. The horizontal axis represents the usual temporal phase oscillation rate $\omega = \partial\beta/\partial t$, and the vertical axis represents the angular phase rotation rate $\alpha = \partial\beta/\partial\varphi$ in a plane perpendicular to the propagation axis of the beam. Since this additional dimension in the frequency is the result of making use of a hitherto unexploited physical property of the electromagnetic field, wireless communication based on angular momentum is fundamentally different from present-day wireless engineering techniques. Hence, it does not require arrays of multiple, spaced antennas or other transducers as is the case for, *e.g.*, the multiple-input-multiple-output (MIMO) technique [82]. Neither does it require massive, power-consuming digital post-processing and has therefore been described as a cost-effective and ‘‘green’’ alternative to MIMO [83].

From a more fundamental physical point of view, the capacity increase made possible by invoking the angular momentum physics layer compared to systems that are based solely on the linear momentum physics layer, is consistent with the fact that all classical fields carry angular momentum [40, 84, 85] and that the dynamics of a physical system is not completely determined unless both its total linear momentum and its total angular momentum are specified [86]. Specifying only one of them is not sufficient. Therefore, utilizing only the linear momentum and not the angular momentum of a system of charges, currents and the pertinent electromagnetic fields is not exploiting such a system to its full capacity.

From the discussion above, it should be clear that in order to ensure not to waste capacity and/or capability in radio science and technology, including radio communications, one must, in addition to the one-dimensional translational degrees of freedom represented by the system's linear momentum, make use also of the mechanical and electromagnetic angular momenta of the system [3, 4, 6, 40, 47–53, 55, 87–91], *i.e.*, the rotational degrees of freedom that are necessary to correctly determine the system's two- and three-dimensional dynamics [92–108].

As is the case for electromagnetic linear momentum, electromagnetic angular momentum can propagate not only in free space, but also in—and interact with—various propagation media [80, 109], including plasma [5, 110–115]. This includes

waveguides [116], and optical fibers [66] where the decay rate, due to absorption, is the same for the angular momentum density as it is for the linear angular momentum density.

III. PHYSICS

In this section we discuss the physics of electromagnetic fields generated by arbitrary, generic sources, and their relation to the electromagnetic observables. In particular, we describe specific properties of the electromagnetic angular momentum observable that sets it apart from the electromagnetic linear momentum observable when it comes to information-carrying capacity for a system with single monolithic transducers (“antennas”) at each end of the link and within a given frequency bandwidth.

A. Electromagnetic fields and observables

Let us consider a finite (source) volume V' that is located in otherwise empty space (free space) and let V' contain an arbitrary distribution of electric charge density $\rho^e(t', \mathbf{x}')$ and electric current density $\mathbf{j}^e(t', \mathbf{x}')$ but no net magnetic charge or current densities ($\rho^m = 0, \mathbf{j}^m = \mathbf{0}$); in conventional radio, V' is the volume in space that is occupied by the transmitting antenna, and $\mathbf{j}^e(t', \mathbf{x}')$ is the conduction current constrained to oscillate along this antenna. The fields produced by the sources in V' propagate to a remotely located observer who uses a sensor of finite volume V to integrate (average) the densities carried by the field at the local time t at the local coordinate \mathbf{x} in V into observables; in conventional radio, V is the volume occupied by the receiving antenna and $\mathbf{j}^e(t, \mathbf{x})$ is the conduction current density constrained to oscillate along this antenna.

The elemental fields $d\mathbf{E}$ and $d\mathbf{B}$ set up at time t in a small volume element d^3x around the point \mathbf{x} in the observation (sensing) volume V originate primarily from the local dynamics at the retarded time t' of the charges and currents in a small volume element d^3x' around the point \mathbf{x}' in the source volume V' . These elemental fields were emitted at the retarded time

$$t' = t'_{\text{ret}}(t, \mathbf{x}, \mathbf{x}') = t - \frac{|\mathbf{x}(t) - \mathbf{x}'(t')|}{c} \quad (22)$$

and propagated to \mathbf{x} along the local unit vector

$$\hat{\mathbf{k}}(\mathbf{x}, \mathbf{x}') = \frac{\mathbf{x} - \mathbf{x}'}{|\mathbf{x} - \mathbf{x}'|} \quad (23)$$

Choosing a convenient gauge, one can readily calculate exact, closed-form generic expressions for the electrodynamic scalar and vector potentials ϕ^e and \mathbf{A}^e . From these potentials it is possible to derive exact expressions for the corresponding generic electromagnetic elemental fields—as well as the fields themselves—directly, without the intermediate step of solving the Maxwell-Lorentz equations from first principles or even calculating the explicit potentials themselves [4, 117–120].

If the sources in V' are at rest (*i.e.*, have no bulk motion) relative to the observation/field point \mathbf{x} (assumed to be at rest

in the lab system, then the elemental fields can be expressed in terms of a non-covariant field vector density $\Theta^e \in \mathbb{R}^3$ as follows:

$$d\mathbf{E}(t, \mathbf{x}, \mathbf{x}') = (d\mathbf{x} \cdot \nabla) \mathbf{E} = d^3x' \Theta^e(t, \mathbf{x}, \mathbf{x}') \quad (24a)$$

$$d\mathbf{B}(t, \mathbf{x}, \mathbf{x}') = (d\mathbf{x} \cdot \nabla) \mathbf{B} = \frac{1}{c} d^3x' (\hat{\mathbf{k}}(\mathbf{x}, \mathbf{x}') \times \Theta^e(t, \mathbf{x}, \mathbf{x}')) \quad (24b)$$

We note that $d\mathbf{E} \perp d\mathbf{B}$ always ($\forall t$) and everywhere ($\forall \mathbf{x}$).

The field vector density Θ^e is a combination of expressions involving the sources ρ^e and \mathbf{j}^e . There are several representations of this combination. Here we choose the representation [6, 121, 122][123]

$$\Theta^e(t, \mathbf{x}, \mathbf{x}') = \sum_{j=1}^4 \mathbf{a}_j^e(t, \mathbf{x}, \mathbf{x}') \quad (25a)$$

where

$$\mathbf{a}_1^e(t, \mathbf{x}, \mathbf{x}') = \frac{1}{\epsilon_0} \frac{\rho^e\left(t - \frac{|\mathbf{x} - \mathbf{x}'|}{c}, \mathbf{x}'\right)}{4\pi|\mathbf{x} - \mathbf{x}'|^2} \hat{\mathbf{k}}(\mathbf{x}, \mathbf{x}') \quad (25b)$$

$$\mathbf{a}_2^e(t, \mathbf{x}, \mathbf{x}') = \frac{1}{\epsilon_0 c} \frac{\mathbf{j}^e\left(t - \frac{|\mathbf{x} - \mathbf{x}'|}{c}, \mathbf{x}'\right) \cdot \hat{\mathbf{k}}(\mathbf{x}, \mathbf{x}')}{4\pi|\mathbf{x} - \mathbf{x}'|^2} \hat{\mathbf{k}}(\mathbf{x}, \mathbf{x}') \quad (25c)$$

$$\mathbf{a}_3^e(t, \mathbf{x}, \mathbf{x}') = \frac{1}{\epsilon_0 c} \frac{\mathbf{j}^e\left(t - \frac{|\mathbf{x} - \mathbf{x}'|}{c}, \mathbf{x}'\right) \times \hat{\mathbf{k}}(\mathbf{x}, \mathbf{x}')}{4\pi|\mathbf{x} - \mathbf{x}'|^2} \times \hat{\mathbf{k}}(\mathbf{x}, \mathbf{x}') \quad (25d)$$

$$\mathbf{a}_4^e(t, \mathbf{x}, \mathbf{x}') = \frac{1}{\epsilon_0 c^2} \frac{\frac{\partial \mathbf{j}^e\left(t - \frac{|\mathbf{x} - \mathbf{x}'|}{c}, \mathbf{x}'\right)}{\partial t} \times \hat{\mathbf{k}}(\mathbf{x}, \mathbf{x}')}{4\pi|\mathbf{x} - \mathbf{x}'|} \times \hat{\mathbf{k}}(\mathbf{x}, \mathbf{x}') \quad (25e)$$

An appealing feature of this representation is that the expressions for the four vectors \mathbf{a}_j do not involve any spatial derivatives, which are known to be cumbersome because of mathematical subtleties due to the retardation that mixes space and time [see Eqn. (22)] as pointed out by Heras [124]. Furthermore, $|\mathbf{a}_j^e|$, $j = 1, 2, 3$, all have a $1/|\mathbf{x} - \mathbf{x}'|^2$ spatial fall-off, whereas $|\mathbf{a}_4^e|$ falls off as $1/|\mathbf{x} - \mathbf{x}'|$ and therefore dominates over the other three at very long distances $|\mathbf{x} - \mathbf{x}'|$ from the source volume V' .

As is well known, it is always possible—and often useful—to decompose a vector \mathbf{v} it into its component \mathbf{v}_{\parallel} parallel to a unit vector $\hat{\mathbf{e}}$, and its component \mathbf{v}_{\perp} transverse to $\hat{\mathbf{e}}$, according to the following scheme:

$$\mathbf{v} = \mathbf{v}_{\parallel} + \mathbf{v}_{\perp} \quad (26a)$$

where

$$\mathbf{v}_{\parallel} = v_{\parallel} \hat{\mathbf{e}} = (\mathbf{v} \cdot \hat{\mathbf{e}}) \hat{\mathbf{e}} \quad (26b)$$

$$\mathbf{v}_{\perp} = \mathbf{v} - \mathbf{v}_{\parallel} = \mathbf{v} - (\mathbf{v} \cdot \hat{\mathbf{e}}) \hat{\mathbf{e}} \quad (26c)$$

We shall use this decomposition several times in the following and start with Θ^e that we write as a sum of one longitudinal

component, Θ_{\parallel}^e , parallel to the unit vector $\hat{\mathbf{k}}$, and one transverse component, Θ_{\perp}^e , perpendicular to $\hat{\mathbf{k}}$, *i.e.*,

$$\Theta^e = \Theta_{\parallel}^e + \Theta_{\perp}^e \quad (27a)$$

where

$$\Theta_{\parallel}^e = \mathbf{a}_1^e + \mathbf{a}_2^e \quad (27b)$$

$$\Theta_{\perp}^e = \mathbf{a}_3^e + \mathbf{a}_4^e \quad (27c)$$

This representation of Θ^e is very convenient when one wishes to calculate and analyze electromagnetic field quantities that are second order in the field vectors.

The local fields $\mathbf{E}(t, \mathbf{x})$ and $\mathbf{B}(t, \mathbf{x})$ at a single field point in the observation volume V are obtained by integrating the contributions from the vector density over the entire source volume V' , *i.e.*, from Eqns. (24) and (25), taking vector perpendicularity into account,

$$\begin{aligned} \mathbf{E}(t, \mathbf{x}) &= \int_{V'} d\mathbf{E} = \int_{V'} d^3x' \Theta^e = \int_{V'} d^3x' (\Theta_{\parallel}^e + \Theta_{\perp}^e) \\ &= \sum_{j=1}^4 \int_{V'} d^3x' \mathbf{a}_j^e(t, \mathbf{x}, \mathbf{x}') \end{aligned} \quad (28a)$$

$$\begin{aligned} \mathbf{B}(t, \mathbf{x}) &= \int_{V'} d\mathbf{B} = \frac{1}{c} \int_{V'} d^3x' (\hat{\mathbf{k}} \times \Theta^e) = \frac{1}{c} \int_{V'} d^3x' (\hat{\mathbf{k}} \times \Theta_{\perp}^e) \\ &= \frac{1}{c} \sum_{j=3}^4 \int_{V'} d^3x' \hat{\mathbf{k}}(\mathbf{x}, \mathbf{x}') \times \mathbf{a}_j^e(t, \mathbf{x}, \mathbf{x}') \end{aligned} \quad (28b)$$

Hence, Θ^e behaves as a volumetric super-density, that, when integrated, yields exact expressions for the fields from which one can, in turn, calculate exact expressions for volumetric densities of the observables that are generated by the sources in V' .

In terms of the Riemann-Silberstein vector (2), the two expressions in Eqns. (24) can be combined into the single complex vector expression

$$d\mathbf{G}(t, \mathbf{x}, \mathbf{x}') = (d\mathbf{x} \cdot \nabla) \mathbf{G} = d^3x' \Theta(t, \mathbf{x}, \mathbf{x}') \quad (29a)$$

where

$$\Theta(t, \mathbf{x}, \mathbf{x}') = \Theta^e(t, \mathbf{x}, \mathbf{x}') + i\hat{\mathbf{k}}(\mathbf{x}, \mathbf{x}') \times \Theta^e(t, \mathbf{x}, \mathbf{x}') \quad (29b)$$

is a vector in \mathbb{C}^3 . Using the decomposition (27), this complex vector can be written

$$\Theta(t, \mathbf{x}, \mathbf{x}') = \Theta_{\parallel}(t, \mathbf{x}, \mathbf{x}') + \Theta_{\perp}(t, \mathbf{x}, \mathbf{x}') \quad (30a)$$

where

$$\Theta_{\parallel}(t, \mathbf{x}, \mathbf{x}') = \Theta_{\parallel}^e(t, \mathbf{x}, \mathbf{x}') \quad (30b)$$

$$\Theta_{\perp}(t, \mathbf{x}, \mathbf{x}') = \Theta_{\perp}^e(t, \mathbf{x}, \mathbf{x}') + i\hat{\mathbf{k}}(\mathbf{x}, \mathbf{x}') \times \Theta_{\perp}^e(t, \mathbf{x}, \mathbf{x}') \quad (30c)$$

Owing to the fact that the real and imaginary parts of the vector Θ_{\perp} are of equal magnitude and perpendicular to each other in

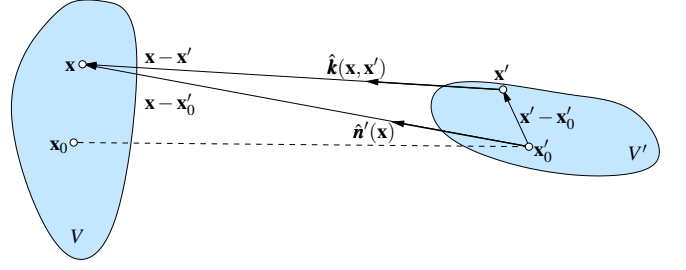


Figure 2. The charges and currents localized in the small volume element d^3x' at the point \mathbf{x}' in the source volume V' around a fixed reference point \mathbf{x}'_0 give rise to elemental fields $d\mathbf{E}(t, \mathbf{x}, \mathbf{x}')$ and $d\mathbf{B}(t, \mathbf{x}, \mathbf{x}')$ in the volume element d^3x at the observation point (field point) \mathbf{x} in the measurement volume V around a fixed reference point \mathbf{x}_0 . These elemental fields propagate along the unit vector of $\mathbf{x} - \mathbf{x}'$ that connects \mathbf{x}' with \mathbf{x} , denoted $\hat{\mathbf{k}}(\mathbf{x}, \mathbf{x}')$. If all individual $\hat{\mathbf{k}}(\mathbf{x}, \mathbf{x}')$ from all individual source points \mathbf{x}' in V' that reach \mathbf{x} are almost parallel, for instance if V' has a small lateral extent as seen from \mathbf{x} (as illustrated), all these unit vectors can be replaced by the \mathbf{x}' independent unit vector $\hat{\mathbf{n}}'(\mathbf{x}) = \hat{\mathbf{k}}(\mathbf{x}, \mathbf{x}'_0)$ that connects \mathbf{x}'_0 with \mathbf{x} . This is the paraxial approximation [120].

\mathbb{R}^3 , it has the following properties:

$$\Theta_{\perp} \cdot \Theta_{\perp} = 0 \quad (31a)$$

$$\Theta_{\perp} \times \Theta_{\perp} = \mathbf{0} \quad (31b)$$

$$\Theta_{\perp} \cdot \Theta_{\perp}^* = 2\Theta_{\perp}^e \cdot \Theta_{\perp}^e = 2(\Theta_{\perp}^e)^2 \quad (31c)$$

$$\Theta_{\perp} \times \Theta_{\perp}^* = 2i(\Theta_{\perp}^e)^2 \hat{\mathbf{k}} - 2i(\Theta_{\perp}^e \cdot \hat{\mathbf{k}}) \Theta_{\perp}^e \quad (31d)$$

We see that Θ_{\perp} behaves as a null (light-cone) vector.

B. Useful approximations

We noticed above that the vector density Θ^e as given by Eqns. (25) has one part, represented by the vectors \mathbf{a}_1 and \mathbf{a}_2 given by Eqns. (25b) and (25c), that is parallel to the unit vector $\hat{\mathbf{k}}$ from a point in the source volume V' to a point in the observation volume V over which the observables are integrated, and another part, represented by the vectors \mathbf{a}_3 and \mathbf{a}_4 in Eqns. (25d) and (25e), that is perpendicular to $\hat{\mathbf{k}}$.

a. The paraxial approximation In a configuration where all the source points \mathbf{x}' in V' are observed at \mathbf{x} in V such that $\hat{\mathbf{k}}(\mathbf{x}, \mathbf{x}')$ are all nearly parallel, the paraxial approximation, illustrated in Fig. 2, can be applied. This amounts to setting

$$\hat{\mathbf{k}}(\mathbf{x}, \mathbf{x}') \approx \hat{\mathbf{k}}(\mathbf{x}, \mathbf{x}'_0) \equiv \hat{\mathbf{n}}'(\mathbf{x}) \quad (32)$$

i.e., approximating the unit vector from \mathbf{x}' to \mathbf{x} with the \mathbf{x} -ward pointing normal unit vector of a sphere centered on a fixed reference point \mathbf{x}'_0 in V' . When we introduce this approximation into the exact expressions for the vectors \mathbf{a}_j^e in Eqns. (25), we

obtain the paraxially approximate vectors

$$\mathbf{a}_1^{\text{e parax}}(t, \mathbf{x}, \mathbf{x}') = \frac{1}{\epsilon_0} \frac{\rho^e\left(t - \frac{|\mathbf{x}-\mathbf{x}'|}{c}, \mathbf{x}'\right)}{4\pi|\mathbf{x}-\mathbf{x}'|^2} \hat{\mathbf{n}}'(\mathbf{x}) \quad (33a)$$

$$\mathbf{a}_2^{\text{e parax}}(t, \mathbf{x}, \mathbf{x}') = \frac{1}{\epsilon_0 c} \frac{\mathbf{j}^e\left(t - \frac{|\mathbf{x}-\mathbf{x}'|}{c}, \mathbf{x}'\right) \cdot \hat{\mathbf{n}}'(\mathbf{x})}{4\pi|\mathbf{x}-\mathbf{x}'|^2} \hat{\mathbf{n}}'(\mathbf{x}) \quad (33b)$$

$$\mathbf{a}_3^{\text{e parax}}(t, \mathbf{x}, \mathbf{x}') = \frac{1}{\epsilon_0 c} \frac{\mathbf{j}^e\left(t - \frac{|\mathbf{x}-\mathbf{x}'|}{c}, \mathbf{x}'\right) \times \hat{\mathbf{n}}'(\mathbf{x})}{4\pi|\mathbf{x}-\mathbf{x}'|^2} \times \hat{\mathbf{n}}'(\mathbf{x}) \quad (33c)$$

$$\mathbf{a}_4^{\text{e parax}}(t, \mathbf{x}, \mathbf{x}') = \frac{1}{\epsilon_0 c^2} \frac{\frac{\partial \mathbf{j}^e\left(t - \frac{|\mathbf{x}-\mathbf{x}'|}{c}, \mathbf{x}'\right)}{\partial t} \times \hat{\mathbf{n}}'(\mathbf{x})}{4\pi|\mathbf{x}-\mathbf{x}'|} \times \hat{\mathbf{n}}'(\mathbf{x}) \quad (33d)$$

These expressions can be further simplified with the help of vector algebraic identities, with the result that the field vector density given by Eqns. (27) can be approximated by

$$\Theta^{\text{e parax}} = \Theta_{\parallel}^{\text{e parax}} + \Theta_{\perp}^{\text{e parax}} \quad (34)$$

If, for compactness, we introduce the overdot ($\dot{\cdot}$) notation

$$\dot{\mathbf{j}}^e \equiv \left(\frac{\partial \mathbf{j}^e}{\partial t} \right)_{t=t'} = \frac{\partial \mathbf{j}^e\left(t - \frac{|\mathbf{x}-\mathbf{x}'|}{c}, \mathbf{x}'\right)}{\partial t} \quad (35)$$

and suppress obvious arguments, then

$$\Theta_{\parallel}^{\text{e parax}} = \frac{c\rho^e \hat{\mathbf{n}}'}{4\pi\epsilon_0 c |\mathbf{x}-\mathbf{x}'|^2} + \frac{(\mathbf{j}^e \cdot \hat{\mathbf{n}}') \hat{\mathbf{n}}'}{4\pi\epsilon_0 c |\mathbf{x}-\mathbf{x}'|^2} \quad (36a)$$

$$\begin{aligned} &\equiv \frac{c\rho^e \hat{\mathbf{n}}'}{4\pi\epsilon_0 c |\mathbf{x}-\mathbf{x}'|^2} + \frac{\mathbf{j}_{\parallel}^e}{4\pi\epsilon_0 c |\mathbf{x}-\mathbf{x}'|^2} \\ \Theta_{\perp}^{\text{e parax}} &= \frac{(\mathbf{j}^e \cdot \hat{\mathbf{n}}') \hat{\mathbf{n}}' - \mathbf{j}^e}{4\pi\epsilon_0 c |\mathbf{x}-\mathbf{x}'|^2} + \frac{(\mathbf{j}^e \cdot \hat{\mathbf{n}}') \hat{\mathbf{n}}' - \mathbf{j}^e}{4\pi\epsilon_0 c^2 |\mathbf{x}-\mathbf{x}'|} \\ &\equiv -\frac{\mathbf{j}_{\perp}^e}{4\pi\epsilon_0 c |\mathbf{x}-\mathbf{x}'|^2} - \frac{\mathbf{j}_{\perp}^e}{4\pi\epsilon_0 c^2 |\mathbf{x}-\mathbf{x}'|} \end{aligned} \quad (36b)$$

Using the above expressions (36), we conclude that in the paraxial approximation the formulas (28) can be approximated by

$$\begin{aligned} \mathbf{E}^{\text{parax}} &= \int_{V'} d^3x' \Theta_{\parallel}^{\text{e parax}} + \int_{V'} d^3x' \Theta_{\perp}^{\text{e parax}} \\ &= \mathbf{E}_{\parallel}^{\text{parax}} + \mathbf{E}_{\perp}^{\text{parax}} \end{aligned} \quad (37a)$$

$$\begin{aligned} \mathbf{B}^{\text{parax}} &= \frac{1}{c} \hat{\mathbf{n}}' \times \int_{V'} d^3x' \Theta_{\perp}^{\text{e parax}} \\ &= \mathbf{B}_{\perp}^{\text{parax}} = \frac{1}{c} \hat{\mathbf{n}}' \times \mathbf{E}_{\perp}^{\text{parax}} = \frac{1}{c} \hat{\mathbf{n}}' \times \mathbf{E}^{\text{parax}} \end{aligned} \quad (37b)$$

Whereas $\mathbf{E}^{\text{parax}}$ has two mutually perpendicular components, $\mathbf{B}^{\text{parax}}$ has only one component. This component is perpendicular both to $\hat{\mathbf{n}}$ and to the component of $\mathbf{E}^{\text{parax}}$ that, in turn, is perpendicular to $\hat{\mathbf{n}}$. These geometrical properties always hold in the paraxial approximation, even if the far-zone approximation is not applicable.

A consistent paraxial approximation expression for the electromagnetic linear momentum density is obtained by inserting the paraxially valid approximate expressions (37) for the fields into the exact expression (A11). The result is

$$\begin{aligned} \mathbf{g}^{\text{field parax}}(t, \mathbf{x}) &= \epsilon_0 (\mathbf{E}_{\parallel}^{\text{parax}} + \mathbf{E}_{\perp}^{\text{parax}}) \times \mathbf{B}_{\perp}^{\text{parax}} \\ &= \mathbf{g}_{\perp}^{\text{field parax}} + \mathbf{g}_{\parallel}^{\text{field parax}} \end{aligned} \quad (38a)$$

where

$$\mathbf{g}_{\perp}^{\text{field parax}}(t, \mathbf{x}) = \epsilon_0 \mathbf{E}_{\parallel}^{\text{parax}} \times \mathbf{B}_{\perp}^{\text{parax}} \quad (38b)$$

$$\mathbf{g}_{\parallel}^{\text{field parax}}(t, \mathbf{x}) = \epsilon_0 E_{\perp}^{\text{parax}} B_{\perp}^{\text{parax}} \hat{\mathbf{n}}' \quad (38c)$$

The angular momentum density carried by $[\mathbf{E}(t, \mathbf{x}), \mathbf{B}(t, \mathbf{x})]$ is given by the exact expression (A38). Inserting the paraxially valid approximate expressions (37) for the fields into (A38), we obtain

$$\begin{aligned} \mathbf{h}^{\text{field parax}}(t, \mathbf{x}; \mathbf{y}) &= (\mathbf{x} - \mathbf{y}) \times \mathbf{g}^{\text{field parax}}(t, \mathbf{x}) \\ &= \mathbf{h}^{\text{field parax}}(t, \mathbf{x}; \mathbf{0}) - \mathbf{y} \times \mathbf{g}^{\text{field parax}}(t, \mathbf{x}) \end{aligned} \quad (39)$$

The first term in the second RHS is the angular momentum around the moment point $\mathbf{y} = \mathbf{0}$

$$\begin{aligned} \mathbf{h}^{\text{field parax}}(t, \mathbf{x}; \mathbf{0}) &= \epsilon_0 \mathbf{x} \times \mathbf{g}_{\perp}^{\text{field parax}} + \epsilon_0 \mathbf{x} \times \mathbf{g}_{\parallel}^{\text{field parax}} \\ &= \epsilon_0 (\mathbf{B}_{\perp}^{\text{parax}} \cdot \mathbf{x}) \mathbf{E}_{\parallel}^{\text{parax}} - \epsilon_0 (\mathbf{E}_{\parallel}^{\text{parax}} \cdot \mathbf{x}) \mathbf{B}_{\perp}^{\text{parax}} \\ &\quad + \epsilon_0 E_{\perp}^{\text{parax}} B_{\perp}^{\text{parax}} \mathbf{x} \times \hat{\mathbf{n}}' \end{aligned} \quad (40)$$

as follows from Eqns. (38) and a well-known vector identity. Recalling that, by definition, the radius vector \mathbf{x} from the source, located at the origin, to the field point is $\mathbf{x} = |\mathbf{x}| \hat{\mathbf{n}}'$, we see that this simplifies to

$$\mathbf{h}^{\text{field parax}}(t, \mathbf{x}; \mathbf{0}) = -\epsilon_0 |\mathbf{x}| E_{\parallel}^{\text{parax}} \mathbf{B}_{\perp}^{\text{parax}} \quad (41)$$

showing that in the paraxial approximation the angular momentum density around the origin depends on the longitudinal component of the electric field vector, is always anti-parallel to the magnetic field vector, and that the bilinear field term is multiplied by a factor that grows linearly with distance $|\mathbf{x}|$ from the source. Using the paraxial relation (37b) and simple vector algebra, we can rewrite Eqn. (41) in the following way:

$$\mathbf{h}^{\text{field parax}}(t, \mathbf{x}; \mathbf{0}) = \frac{\epsilon_0}{c} (\mathbf{x} \cdot \mathbf{E}_{\parallel}^{\text{parax}} \otimes \mathbf{E}_{\perp}^{\text{parax}}) \times \hat{\mathbf{n}}' \quad (42)$$

where \otimes is the dyadic product operator.

In a spherical polar coordinate system (r, ϑ, φ) where $\mathbf{x} = r\hat{\mathbf{r}}$ and $\hat{\mathbf{r}} = \hat{\mathbf{n}}'$ we obtain

$$\mathbf{h}^{\text{field parax}}(t, r, \vartheta, \varphi; \mathbf{0}) = -\epsilon_0 r E_r^{\text{parax}} \mathbf{B}_{\perp}^{\text{parax}} \quad (43)$$

The longitudinal (radial) part of the electric field $E_{\parallel} = E_r$ falls off as $1/r^2$ and the transverse magnetic field B_{\perp} falls off as $1/r$, which means that their product falls off as $1/r^3$. But since the formula contains a factor r multiplying the product

of the fields that precisely compensates for the faster fall off of $E_{\parallel} = E_r$, the angular momentum density, to leading order in r , always falls off as $1/r^2$. This result is generally valid for radiation from arbitrary charge and/or current distributions ρ^e and \mathbf{j}^e . It is valid for small and large beam widths alike, for any beam shape, form and direction, and for sensor volumes of any (finite) size and shape, even for antennas that intercept only a fraction of the beam [45, 62, 121].

b. The far-zone approximation In the far-zone approximation, the integrands (27) and (36) can be consistently approximated in order to further simplify the integrals (28) and (37), respectively. With reference to Fig. 2, and with the choice of the reference point \mathbf{x}'_0 as the origin of the spherical polar coordinate used, implying that

$$\mathbf{x} - \mathbf{x}'_0 = \mathbf{r} = r\hat{\mathbf{r}} \quad (44a)$$

$$\mathbf{x}' - \mathbf{x}'_0 = \mathbf{r}' = r'\hat{\mathbf{r}}' \quad (44b)$$

the identity

$$\frac{1}{|\mathbf{x} - \mathbf{x}'|} = \frac{1}{|(\mathbf{x} - \mathbf{x}'_0) - (\mathbf{x}' - \mathbf{x}'_0)|} = \frac{1}{|\mathbf{r} - \mathbf{r}'|} \quad (45)$$

holds. For configurations such that the shortest distance between V' and V is large, or, more precisely,

$$\sup r' = \sup |\mathbf{x}' - \mathbf{x}'_0| \ll \inf |\mathbf{x} - \mathbf{x}'_0| = \inf r \quad (46)$$

the Taylor expansion

$$\begin{aligned} \frac{1}{|\mathbf{x} - \mathbf{x}'|} &= \frac{1}{|\mathbf{r} - \mathbf{r}'|} \\ &= \frac{1}{r} - (\mathbf{r}' \cdot \nabla) \frac{1}{r} - \frac{1}{2} (\mathbf{r}' \cdot \nabla)^2 \frac{1}{r} + \dots \\ &= \frac{1}{r} + \frac{\mathbf{r}' \cdot \hat{\mathbf{r}}}{r^2} + \frac{1}{2} \frac{\hat{\mathbf{r}} \cdot (3\mathbf{r}' \otimes \mathbf{r}' - \mathbb{1}_3 r'^2) \cdot \hat{\mathbf{r}}}{r^3} + \mathcal{O}(r^{-4}) \end{aligned} \quad (47)$$

converges rapidly. This allows us to set $1/|\mathbf{x} - \mathbf{x}'| \approx 1/r$ in Eqns. (36). As a result, the un-truncated expressions for the longitudinal and transverse components of the field density vector in the combined paraxial and far-zone approximations can be written

$$\Theta_{\parallel}^e \text{paraxfar} = \frac{c\rho^e \hat{\mathbf{n}}'}{4\pi\epsilon_0 cr^2} + \frac{\mathbf{j}_{\parallel}^e}{4\pi\epsilon_0 cr^2} \quad (48a)$$

$$\Theta_{\perp}^e \text{paraxfar} = -\frac{\mathbf{j}_{\perp}^e}{4\pi\epsilon_0 cr^2} - \frac{\dot{\mathbf{j}}_{\perp}^e}{4\pi\epsilon_0 c^2 r} \quad (48b)$$

Accordingly, the integrals in Eqns. (37) simplify considerably.

Following Tamburini *et al.* [62] and Thidé *et al.* [121], we introduce the following shorthand notations:

$$q^e(t') \equiv \int_{V'} d^3x' \rho^e(t', \mathbf{x}') \quad (49)$$

$$\mathbf{I}^e(t') \equiv \int_{V'} d^3x' \mathbf{j}^e(t', \mathbf{x}') \quad (50)$$

$$\begin{aligned} \dot{\mathbf{I}}^e(t') &\equiv \int_{V'} d^3x' \dot{\mathbf{j}}^e(t', \mathbf{x}') \\ &\equiv \int_{V'} d^3x' \frac{\partial \mathbf{j}^e(t - \frac{|\mathbf{x} - \mathbf{x}'|}{c}, \mathbf{x}')}{\partial t} \end{aligned} \quad (51)$$

Then, under the assumption of paraxial as well as far-zone approximation, we can write the parallel and perpendicular components of the fields as follows:

$$\mathbf{E}_{\parallel}^{\text{paraxfar}} = \frac{cq^e(t')\hat{\mathbf{n}}'}{4\pi\epsilon_0 cr^2} + \frac{\mathbf{I}_{\parallel}^e}{4\pi\epsilon_0 cr^2} \quad (52a)$$

$$\mathbf{E}_{\perp}^{\text{paraxfar}} = -\frac{\mathbf{I}_{\perp}^e}{4\pi\epsilon_0 cr^2} - \frac{\dot{\mathbf{I}}_{\perp}^e}{4\pi\epsilon_0 c^2 r} \quad (52b)$$

$$\mathbf{B}_{\perp}^{\text{paraxfar}} = \frac{\mathbf{I}_{\perp}^e \times \hat{\mathbf{n}}'}{4\pi\epsilon_0 cr^2} + \frac{\dot{\mathbf{I}}_{\perp}^e \times \hat{\mathbf{n}}'}{4\pi\epsilon_0 c^2 r} \quad (52c)$$

Evaluating the linear momentum density formula (A10) in the paraxial approximation, keeping all terms and approximating each one in a consistent way, we find that far away from the source the linear momentum density is given by the accurate formula

$$\mathbf{g}^{\text{fieldparaxfar}} = \mathbf{g}_{\perp}^{\text{fieldparaxfar}} + \mathbf{g}_{\parallel}^{\text{fieldparaxfar}} \quad (53a)$$

where the approximate, but un-truncated expressions

$$\mathbf{g}_{\perp}^{\text{fieldparaxfar}} = \frac{cq^e(t') + I_{\parallel}^e(t')}{16\pi^2\epsilon_0 c^2 r^3} \left(\frac{\mathbf{I}_{\perp}^e}{r} + \frac{\dot{\mathbf{I}}_{\perp}^e}{c} \right) \quad (53b)$$

$$\mathbf{g}_{\parallel}^{\text{fieldparaxfar}} = \frac{1}{16\pi^2\epsilon_0 c^2 r^2} \left| \frac{\mathbf{I}_{\perp}^e}{r} + \frac{\dot{\mathbf{I}}_{\perp}^e}{c} \right|^2 \hat{\mathbf{n}}' \quad (53c)$$

can be used.

If we express this result in terms of the integrals in Eqns. (37), we find that as the distance r from the source tends to infinity, then, to leading order in r , the linear momentum density vector is given by the truncated expression

$$\begin{aligned} \mathbf{g}^{\text{fieldparaxfar}} &= \frac{1}{16\pi^2\epsilon_0 c^4 r^3} \left(\int_{V'} d^3x' (c\rho^e + \mathbf{j}_{\parallel}) \right. \\ &\quad \times \left. \int_{V'} d^3x' \left(\frac{\partial \mathbf{j}^e(t', \mathbf{x}')}{\partial t} \right)_{\perp} + \mathcal{O}(r^{-4}) \right) \\ &\quad + \frac{1}{16\pi^2\epsilon_0 c^4 r^2} \left(\left| \int_{V'} d^3x' \left(\frac{\partial \mathbf{j}^e(t', \mathbf{x}')}{\partial t} \right)_{\perp} \right|^2 \right. \\ &\quad \left. + \mathcal{O}(r^{-3}) \right) \hat{\mathbf{n}}' \end{aligned} \quad (54)$$

To leading order in r the magnitude of this vector is the scalar

$$\left| \mathbf{g}^{\text{fieldparaxfar}} \right| = \frac{1}{16\pi^2\epsilon_0 c^4 r^2} \left| \int_{V'} d^3x' \left(\frac{\partial \mathbf{j}^e(t', \mathbf{x}')}{\partial t} \right)_{\perp} \right|^2 + \mathcal{O}(r^{-3}) \quad (55)$$

a well-known formula exhibiting the expected r^{-2} fall-off. We note that the magnitude of the far-zone linear momentum density [and thereby also the far-zone Poynting vector; see Eqn. (A12)] has, to leading order in r , a simple dependence on the sources, being completely determined by one source integral only, and therefore by (the asymptotic approximation of) the single term \mathbf{a}_4^e of the sum in expression (25).

Evaluating the un-truncated expression for the angular momentum density, Eqn. (A37), in the paraxial approximation, and far away from the source, is trickier. Noticing that $\mathbf{x} = r\hat{\mathbf{n}}'$, we see that the angular momentum density *cannot* be obtained from the longitudinal part of the linear momentum density (53c) that is the dominating one in the far zone because the vector product with \mathbf{x} would yield zero. Instead we have to use Eqn. (43) to obtain the un-truncated expression

$$\mathbf{h}^{\text{fieldparaxfar}}(\mathbf{0}) = -\frac{cq^e(t') + J_{\parallel}^e(t')}{16\pi^2\epsilon_0c^2r^2} \left(\frac{\mathbf{I}_{\perp}^e}{r} + \frac{\mathbf{I}_{\parallel}^e}{c} \right) \times \hat{\mathbf{n}}' \quad (56)$$

Expressing this result explicitly in the integrals in Eqns. (37), and truncating consistently, we obtain

$$\mathbf{h}^{\text{fieldparaxfar}}(\mathbf{0}) = \frac{1}{16\pi^2\epsilon_0c^4r^2} \hat{\mathbf{n}}' \times \left(\int_{V'} d^3x' (c\rho^e + \mathbf{j}_{\parallel}) \right. \\ \left. \times \int_{V'} d^3x' \left(\frac{\partial \mathbf{j}^e(t', \mathbf{x}')}{\partial t} \right)_{\perp} + \mathcal{O}(r^{-3}) \right) \quad (57)$$

As can be seen, the magnitude of the angular momentum density has an r^{-2} asymptotic fall-off [see also Table II and Abraham [45], Tamburini *et al.* [62], and Thidé *et al.* [121]], but the expression (56), involving four source integrals, is considerably more complicated than the corresponding approximate expression (54) for the linear momentum density. We also see that far away from V' , the dominating contribution to the magnitude of the linear momentum density (Poynting vector) comes from the asymptotic approximation of the far-zone \mathbf{a}_4^e term in the integrands in Eqns. (28) for \mathbf{E} and \mathbf{B} . However, the dominating contribution to the magnitude of the angular momentum in the same region comes from the *near-zone* \mathbf{a}_1^e and \mathbf{a}_2^e terms for \mathbf{E} and the *far-zone* \mathbf{a}_4^e term for \mathbf{B} . Hence, as was shown by Then and Thidé [103], the far-zone \mathbf{E} field has in general no influence on the far-zone angular momentum as was shown by Then and Thidé [103]. This may at first seem like a paradox but is a fact that was established already a century ago by Abraham [45]; see also Then and Thidé [103] and Tamburini *et al.* [62]. Hence, whereas it is easy to use far-zone data to modify the properties of the far-zone linear momentum density in a feedback manner, it is quite cumbersome to do the same for the angular momentum density.

IV. IMPLEMENTATION

For many reasons, not least to overcome the problem of frequency congestion, it is desirable to strive for a more resource-conserving, efficient and flexible use of the electromagnetic field in radio science, radar, and wireless communication applications than is possible with the prevalent linear-momentum techniques. Furthermore, it is usually easier to achieve a high degree of coherence and phase accuracy at radio wavelengths than at optical ones. Hence, as pointed out in Thidé *et al.* [57], it is often more convenient to perform fundamental studies of electromagnetic radiation, including those addressed in this article, in radio than in optics. In this Section we discuss physical issues that are essential to consider when developing

and implementing angular momentum techniques in the radio domain.

Let us consider a spatially limited source volume V' from which an electromagnetic beam is emitted during a finite time interval Δt into free space where there is no creation or annihilation of neither linear nor angular field momentum. As shown in Sect. III, a sufficiently long time t_0 after the end of this signal “pulse” has left the source region it will be propagating radially outward with speed c into the surrounding free space and be located in a finite volume V_0 between two spherical shells, one with radius $r_0 = ct_0$ relative to a reference point \mathbf{x}'_0 in V' (see Fig. 2), and another with radius $r_0 + \Delta r_0$ where $\Delta r_0 = c\Delta t$ [3]. According to the conservation laws (A22) and (A49), the field momentum $\mathbf{p}^{\text{field}}$ and angular momentum $\mathbf{J}^{\text{field}}$ contained in this spatially limited volume do not fall off asymptotically at large distances from the source.

Consequently, both linear and angular electromagnetic field momenta can propagate—and be used for information transfer—over in principle arbitrarily long distances. Of course, the magnitude and angular distribution of the respective momentum densities depend on the specific spatio-temporal and topological properties of the actual radiating and receiving transducers (“antennas”) used. Some transducers, such as linear dipoles and similar one-dimensional antennas used in radio today, are effective radiators and sensors of linear momentum, whereas well-defined coherent superpositions of angular momentum eigenmodes are more optimally radiated and sensed by transducers making full use of two- or three-dimensional current distributions.

A. Wireless information transfer using linear momentum

If we identify the individual terms in the global law of conservation of linear momentum in a closed volume, (A22), we can rewrite this equation as a balance equation between the time rate change of mechanical linear momentum, *i.e.*, the force on the matter (the charged mechanical particles) in V , the time rate change of field linear momentum in V , and the flow of field linear momentum into V as follows:

$$\underbrace{\int_V d^3x \mathbf{f}}_{\text{Force on the matter}} + \frac{d}{dt} \underbrace{\int_V d^3x \epsilon_0 (\mathbf{E} \times \mathbf{B})}_{\text{Field momentum}} + \underbrace{\oint_S d^2x \hat{\mathbf{n}} \cdot \mathbf{T}}_{\text{Linear momentum flow}} = \mathbf{0} \quad (58)$$

Hence, electric charges that are subject to an oscillating EMF from a transmitter, fed into an antenna via a transmission line, experience a mechanical force. This mechanical force sets these charges into translational motion and therefore gives rise to a time-varying linear conduction current density $\mathbf{j}^e(t', \mathbf{x}')$ in V' . The conservation law (A22) also shows that $\mathbf{j}^e(t', \mathbf{x}')$ is accompanied by the simultaneous emission of a time-varying electromagnetic field linear momentum $\mathbf{p}^{\text{field}}(t)$ that propagates in free space away from V' in the form of the linear momentum density $\mathbf{g}^{\text{field}}(t, \mathbf{x}')$, as described in earlier Sections and in Appendix A.

For illustrative purposes, let us consider an electromechanical system of fields interacting with point charges q_i , $i = 1, 2, \dots, j, \dots, n$, located at \mathbf{x}_i at time t_i . All charges have

the same charge q and same mass m . The charge density ρ_j^e representing the j th point charge q_j at \mathbf{x}_j can be described in the form of the Dirac delta distribution

$$\rho_j^e = q\delta(\mathbf{x} - \mathbf{x}_j) \quad (59)$$

We then find that the Lorentz force acting on q_j due to the Maxwell stresses is

$$\begin{aligned} \mathbf{F}_j \equiv \mathbf{F}(t_j, \mathbf{x}_j) &= \int_V d^3x \mathbf{f} = \int_V d^3x \rho_j^e (\mathbf{E} + \mathbf{v}^{\text{mech}} \times \mathbf{B}) \\ &= q\mathbf{E}(t_j, \mathbf{x}_j) + q\mathbf{v}^{\text{mech}}(t_j, \mathbf{x}_j) \times \mathbf{B}(t_j, \mathbf{x}_j) \quad (60) \\ &\equiv q\mathbf{E}_j + q\mathbf{v}_j^{\text{mech}} \times \mathbf{B}_j = q\mathbf{E}_j + \mathbf{j}_j^e \times \mathbf{B}_j \end{aligned}$$

Expressed in the mechanical linear momentum of particle j , $\mathbf{p}_j^{\text{mech}}$, this can be written

$$\frac{d\mathbf{p}_j^{\text{mech}}}{dt} - \frac{q}{m} \mathbf{p}_j^{\text{mech}} \times \mathbf{B}_j = q\mathbf{E}_j \quad (61)$$

This illustrates that the process of estimating the fields from the measured current in a linear antenna of finite one-dimensional extent where the charges experience a holonomic constraint is difficult and can only be projective. The situation gets worse if we also include self-interaction effects, re-radiation, pre-acceleration and related complications [55, Supplement].

In a remote volume V that also contains electric charges, the conservation law (A22) shows that the reverse process takes place in that (a part of) the flow of field linear momentum density $\mathbf{g}^{\text{field}}(t, \mathbf{x})$ emitted from V' is integrated in V into a field linear momentum $\mathbf{p}^{\text{field}}(t)$ that is accompanied by a mechanical linear momentum $\mathbf{p}^{\text{mech}}(t)$. This gives rise to a translational motion of the charges and, hence, a translational (non-rotational) conduction current. If V is a very thin cylindrical conductor, as in typical radio communications scenarios, this is a one-dimensional, scalar, conduction current, called the ‘‘antenna current’’, that is fed to the receiving equipment through a transmission line. Clearly, such a linear receiving antenna system senses the electromagnetic linear momentum carried by the radio beam but cannot sense the electromagnetic angular momentum carried by the same beam. As we have seen, this technique, on which most of today’s radio science and communication applications rests, is based on the linear momentum physical layer.

When the fields are emitted from a localized source, *e.g.*, a typical transmitting antenna, it is convenient to evaluate the integral in the right-hand member of Eqn. (A19), determining the field linear momentum in a volume away from V' , in a spherical polar coordinate system (r, ϑ, φ) with its origin at the center of the source region, *e.g.*, the antenna phase center. Consequently, the total linear momentum carried by such an electromagnetic ‘‘pulse’’ of finite duration δt is

$$\mathbf{p}^{\text{field}}(t) = \int_{r_0}^{r_0 + \Delta r_0} dr r^2 \int_0^{2\pi} d\varphi \int_0^\pi d\vartheta \sin \vartheta \mathbf{g}^{\text{field}}(t, r, \vartheta, \varphi) \quad (62)$$

when it propagates in free space [3]. The integration over the angular domain (the two last integrals) yields a function of r

(and t) that, for very large $r_0 = ct_0$, becomes proportional to r^{-2} as shown by expressions (53) and (54).

Taking into account that this function shall in the remaining (*i.e.*, first) integral in the right-hand member of Eqn. (62) be first multiplied by r^2 and thereafter integrated over the finite radial interval $[r_0, r_0 + \Delta r_0] \equiv [ct_0, c(t_0 + \Delta t)]$, we see that $|\mathbf{p}^{\text{field}}|$ tends to a constant when r_0 tends to infinity. This asymptotic independence of distance from a localized source, allowing the field linear momentum generated by this source to be transported all the way to infinity without radial fall-off and therefore be irreversibly lost there, is the celebrated arrow of radiation asymmetry (see Eddington [125, pp. 328–329], Jackson [4, Chap. 6], Zeh [126], and Rohrlich [55, Chap. 9]).

The angular distribution in the far zone of the magnitude of the linear momentum density, $|\mathbf{g}^{\text{fieldfar}}|$ and, consequently, of the Poynting vector $|\mathbf{S}|$ [see relation (A12)], is usually called ‘‘the radiation pattern’’ or, in the case of antenna engineering, ‘‘the antenna pattern’’ or ‘‘antenna diagram’’.

B. Wireless information transfer using angular momentum

As the global law of conservation of angular momentum in a closed volume, Eqn. (A49), shows, the electric charges in a source volume V' that are subject to a time-varying surface integrated angular momentum flux \mathbf{M} suffer a change in their total mechanical angular momentum \mathbf{h}^{mech} , *i.e.*, a mechanical torque $\boldsymbol{\tau}^{\text{mech}}$. This mechanical torque sets these charges into two- or three-dimensional rotational motion that causes the emission of a superposition of electromagnetic angular momentum eigenmodes that propagates in free space away from V' in the form of the angular momentum density $\mathbf{h}^{\text{field}}$ as described in earlier Sections and in Appendix A.

Eqn. (A49) can be written in the form of a balance equation between the time rate change of mechanical torque on the matter in V (the charged mechanical particles), the time rate change of field angular momentum and the flow of angular momentum across the surface S , which encloses V , as follows:

$$\underbrace{\int_V d^3x \boldsymbol{\tau}(\mathbf{y})}_{\text{Torque}} + \frac{d}{dt} \underbrace{\int_V d^3x (\mathbf{x} - \mathbf{y}) \times \varepsilon_0 (\mathbf{E} \times \mathbf{B})}_{\text{Field angular momentum}} + \underbrace{\oint_S d^2x \hat{\mathbf{n}} \cdot \mathbf{M}}_{\text{Angular momentum flow}} = \mathbf{0} \quad (63)$$

For illustrative purposes we consider the j th charge q_j in a system of n point charges $q_i, i = 1, 2, \dots, j, \dots, n$, each carrying the charge q . The charge density can be represented by the Dirac delta distribution as given by Eqn. (59). Then we find that the mechanical torque on q_j is

$$\begin{aligned} \boldsymbol{\tau}_j \equiv \boldsymbol{\tau}(t_j, \mathbf{x}_j; \mathbf{y}) &= \int_V d^3x (\mathbf{x} - \mathbf{y}) \times \mathbf{f} \\ &= \int_V d^3x (\mathbf{x} - \mathbf{y}) \times (\rho_j^e \mathbf{E} + \mathbf{j}^e \times \mathbf{B}) \quad (64) \\ &= (\mathbf{x}_j - \mathbf{y}) \times \mathbf{F}_j \end{aligned}$$

where \mathbf{F}_j is the Lorentz force on q_j , given by Eqn. (60).

In a remote observation volume V containing charges that can move freely in all directions, the reverse process takes place

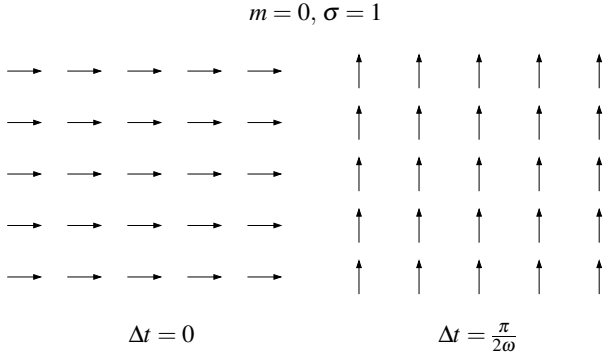


Figure 3. Schematic plot of the instantaneous directions of the field vectors in a left-hand circular polarized cylindrical beam (SAM $\sigma = 1$), projected onto the phase plane perpendicular to the z axis (pointing out of the figure). The right-hand panel shows the situation 1/4 period later than the left-hand panel. The beam does not carry OAM so the directions of the field vectors vary only with time and rotate in unison.

in that (a part of) the flow of field angular momentum density emitted from V' is intercepted and integrated into a mechanical angular momentum \mathbf{J}^{mech} . This gives rise to a rotational motion of the charges and, hence, to a two- or three-dimensional rotational (non-translational) current density in V . Therefore, a receiving antenna for electromagnetic angular momentum carried by a radio beam must be a transducer that can detect the vectorial property of the current density and therefore must be two- or three-dimensional; a one-dimensional linear antenna of the type discussed in the previous subsection can only detect linear momentum. Applications that use the angular momentum degrees of freedom must therefore be implemented in techniques that are based on the angular momentum physical layer.

The field angular momentum about the origin, $\mathbf{J}^{\text{field}}(\mathbf{0})$, contained in the “pulse” emitted from the same localized source and volume as described by equation (62), is

$$\mathbf{J}^{\text{field}}(t, \mathbf{0}) = \int_{r_0}^{r_0 + \Delta r_0} dr r^2 \int_0^{2\pi} d\varphi \int_0^\pi d\vartheta \sin \vartheta \mathbf{h}^{\text{field}}(t, r, \vartheta, \varphi) \quad (65)$$

The expressions (56) and (57) explicitly show that the angular momentum density $\mathbf{h}^{\text{field}}$ emitted from any electromagnetic radiation source has precisely the same asymptotic r^{-2} radial fall-off in all directions as the linear momentum density $\mathbf{g}^{\text{field}}$. Hence, it is clear that also $|\mathbf{J}^{\text{field}}|$ tends asymptotically to a constant value and is irreversibly lost when the “pulse” approaches infinity. This is the angular momentum analog of the linear momentum arrow of radiation.

We point out that for one and the same radiating device (“antenna”), the angular distribution of the radiated *angular* momentum density $|\mathbf{h}^{\text{field}}|$ is quite different from the angular distribution of the radiated *linear* momentum density, $|\mathbf{g}^{\text{field}}|$; see Eqns. (53) and (56), Thid *et al.* [5], and Then and Thid [103].

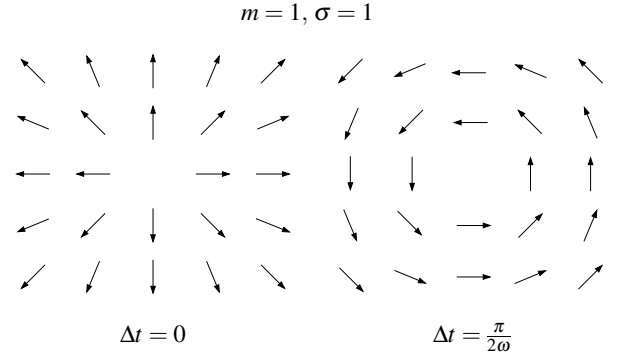


Figure 4. Same as Fig. 3, but for the case that the beam also carries a z component of OAM, L_z , with azimuthal quantum number (mode index) $m = 1$, corresponding to a phase variation $e^{i\varphi}$ of the field where φ is the azimuth angle around the z axis. As a result, the instantaneous direction of the field vector depends on φ in addition to varying with time due to SAM.

1. Spin angular momentum (SAM) vs. orbital angular momentum (OAM)

It is shown in Subsection A3 in Appendix A, that if the vector potential \mathbf{A} fulfills the criteria for Helmholtz decomposition, it is possible to separate the analytic expression for the total field angular momentum, $\mathbf{J}^{\text{field}}$, into two exact, gauge independent expressions. One that is not dependent of the moment point, Σ^{field} , *viz.*, expression (A51a), and one that is, $\mathbf{L}^{\text{field}}$, *viz.*, expression (A51b). In radio communication scenarios these expressions can be identified with the spin and angular momentum, respectively, of the radio beam.

Figure 3 illustrates how the intrinsic spin part of the angular momentum (SAM), Σ^{field} , manifests itself as a unison rotation in time of the field vectors such that they all have one and the same direction across the phase front of the beam at given time t , and all have rotated into another direction (modulo 2π in oscillation frequency phase ωt) in each point at time $t + \Delta t$. Hence, the measurement of SAM (polarization) requires temporal coherence.

A common technique to observe and exploit SAM in radio is to use two co-located linear dipole antennas arranged orthogonally to each other and to determine the polarization state by comparing the phases of the antenna currents induced in the two antennas by using interferometry. In antenna engineering such antennas are known as turnstile antennas [99, 108, 127]. Another technique is to use longitudinal mode helical antennas; see Someda [128, example 12.7.1, p. 461].

In contrast to SAM, the orbital part of the electrodynamic angular momentum, the orbital angular momentum (OAM), $\mathbf{L}^{\text{field}}$, is an extrinsic (coordinate dependent) property. Figure 4 illustrates how OAM manifests itself as a rotation in space of the field vectors such that they at any given instant have different directions (modulo 2π in oscillation frequency phase ωt) for different azimuth angles positions φ and $\varphi + \Delta\varphi$ around the z (beam) axis in the phase plane. Hence, the measurement of OAM requires spatial coherence.

As the conservation law (A49) shows, angular-momentum

radio beams should ideally be radiated and sensed by “antennas” based on torque action [92–108], *i.e.*, transducers allowing the particles move and currents to flow freely in all directions, rather than in only one direction as in linear antennas of a dipole type that are based on force action (1D translational oscillations/rectilinear acceleration of charges; antenna currents). Interesting possibilities to develop monolithic transducers that can generate and sense SAM and OAM are offered by optomechanics [108, 129–132], spintronics [133, 134], and orbitronics [135, 136].

Since the direct generation and detection of angular momentum modes requires transducers that are based on rotational degrees of freedom and torque, they must in general allow three-dimensional currents. If, however, the rotation is confined to a single plane, it suffices that the transducers are two-dimensional. Such “antennas” are not yet readily available for the radio frequency range. However, spatially distributed phased arrays of linear-momentum antennas used in today’s radio astronomy and wireless communications, *e.g.*, MIMO, spatially sample a radio beam in discrete points and therefore can approximate, within the limitations and constraints set by the sampling theorem, the properties of a continuous two- and three-dimensional transducer. Hence, such arrays can be used for analyzing and synthesizing a finite subset of the OAM eigenmodes and coherent superpositions thereof [57]. This makes it possible to use currently available radio equipment and techniques for experimental investigations of certain properties of electromagnetic angular momentum. These experiments amount to measuring the 1D translational currents, *i.e.* one component of the linear momentum of the charges, in the individual antenna elements over a plane and then performing a phase gradient analysis [5, 77, 91, 137–140] and post-processing the data so that the approximate (and possibly aliased) spectrum of the z component of the angular momentum, L_z can be estimated and the individual OAM eigenmodes be extracted and an approximation of the correct spectrum of individual OAM eigenmodes and the information they carry be decoded. It should be emphasized that this way of estimating L_z is based on the application of the operator in (A53c) on the electric (or magnetic) field, which, as was discussed in Sect. II, is not directly observable. Investigations of the properties of OAM using available array antennas pave the way for the development of future innovative angular momentum radio concepts.

Whereas it is *possible* to use arrays of conventional linear-momentum antennas (*e.g.*, dipole antennas) to enable exploitation of a small set of angular momentum modes in applications, it is not *necessary* to do so. It should also be emphasized that for EM beams of the kind used in radio astronomy, radar investigations, radio communications and similar applications, OAM is distinctively different from—and independent of—SAM (wave polarization). If such a beam is already N -fold OAM encoded, utilizing also SAM will double the information transfer capacity by virtue of the fact that the dimension of the state space then doubles from N to $2N$.

2. Electric dipoles

A very common antenna type in radio is the half-wavelength dipole. Many qualitative as well as quantitative characteristics of this antenna are fairly accurately approximated by an electric Hertzian dipole, *i.e.*, an antenna whose length L is much shorter than the wavelength λ of its emitted (nearly monochromatic) field, $L \ll \lambda$, so that the phase of the antenna current can be considered constant over L , a condition that simplifies the analysis considerably. Let us therefore calculate analytically the linear and angular momentum densities emitted by a single Hertzian dipoles and combinations of such dipoles. We choose a Cartesian coordinate system (x_1, x_2, x_3) where the x_3 axis coincides with the polar axis of a spherical polar coordinate system (r, ϑ, φ) and let the two systems have the same origin $\mathbf{x}' = \mathbf{0}$.

a. Single Hertzian dipole The properties of Hertzian dipoles are described in many textbooks [4, 6, 40] and explicit formulas are derived in Appendix B.

According to Eqn. (B17) for $\mathbf{E}_3 \times \mathbf{B}_3$ the electromagnetic linear momentum density, $\mathbf{g}_3^{\text{field}} = \epsilon_0 \mathbf{E}_3 \times \mathbf{B}_3$, emitted from a single Hertzian dipole $\mathbf{d}_3(\mathbf{0})$ located at the origin and directed along the x_3 axis, has nine different vector components. Five of them are longitudinal ($\parallel \hat{\mathbf{r}}$) and four of them are transverse ($\perp \hat{\mathbf{r}}$). It follows trivially from Planck’s relation, Eqn. (A12), that the same is also true for the Poynting vector \mathbf{S} . However, the different components have different fall-offs, implying that far away from the dipole the following approximation holds:

$$\begin{aligned} \mathbf{g}_3^{\text{field}^{\text{far}}}(t, r, \vartheta, \varphi) &= \frac{k^4 d_3^2}{32\pi^2 \epsilon_0 c} \left(\frac{1 + \cos[2(kr - \omega t + \delta_3)]}{r^2} + \mathcal{O}(r^{-3}) \right) \sin^2 \vartheta \hat{\mathbf{r}} \\ &+ \frac{k^3 d_3^2}{32\pi^2 \epsilon_0 c} \left(\frac{\sin[2(kr - \omega t + \delta_3)]}{r^3} + \mathcal{O}(r^{-4}) \right) \cos 2\vartheta \hat{\boldsymbol{\vartheta}} \end{aligned} \quad (66)$$

To the same degree of approximation, the cycle (temporal) average of the Poynting vector in the far zone is, to leading order,

$$\langle \mathbf{S}_3^{\text{far}} \rangle_t = c^2 \mathbf{g}_3^{\text{field}^{\text{far}}} \approx \frac{\omega^4 d_3^2}{32\pi^2 \epsilon_0 c^3} \left(\frac{1}{r^2} + \mathcal{O}(r^{-3}) \right) \sin^2 \vartheta \hat{\mathbf{r}} \quad (67)$$

where we used the fact that $k = \omega/c$ and that

$$\langle \sin[2(kr - \omega t + \delta_3)] \rangle_t = \langle \cos[2(kr - \omega t + \delta_3)] \rangle_t = 0 \quad (68)$$

This is a well-known result that can be found in most textbooks.

To calculate the electromagnetic angular momentum density around $\mathbf{y} = \mathbf{0}$ we use Eqn. (A37), Eqn. (B17), and the fact that $\mathbf{x} = r\hat{\mathbf{r}}$ and $\hat{\mathbf{r}} \times \hat{\boldsymbol{\vartheta}} = -\hat{\boldsymbol{\varphi}}$ to obtain the exact expression

$$\begin{aligned} \mathbf{h}_3^{\text{field}}(t, r, \vartheta, \varphi; \mathbf{0}) &= r\hat{\mathbf{r}} \times \mathbf{g}_3^{\text{field}} = \frac{d_3^2}{8\pi^2 \epsilon_0 c} r [f_1(\delta_3) f_2(\delta_3) \\ &- f_2^2(\delta_3) + f_1(\delta_3) f_3(\delta_3) - f_2(\delta_3) f_3(\delta_3)] \sin \vartheta \cos \vartheta \hat{\boldsymbol{\varphi}} \end{aligned} \quad (69)$$

where the functions f_n are given by Eqns. (B12).

At very long distances from a Hertzian dipole located at the origin and oscillating along the x_3 axis we can use the approximation in Eqn. (66) for $\mathbf{g}_3^{\text{field}}$. Because of the geometry, only the transverse part ($\perp \hat{\mathbf{r}}$) of the linear momentum density, where the dominating part is $\mathcal{O}(r^{-3})$, contributes to the linear momentum density in the far zone. The radial component ($\parallel \hat{\mathbf{r}}$) of the linear momentum density (Poynting vector), which is $\mathcal{O}(r^{-2})$ does not contribute to the angular momentum density. If it would, then expression (65) for the total angular momentum at very large distances of a ‘‘pulse’’ would grow without bounds as the ‘‘pulse’’ propagates, thus violating fundamental laws of physics such as the conservation of energy. See the detailed, clarifying discussion about this by Abraham [45]; an English translation of the essential part of this discussion is included in Tamburini *et al.* [62]. This almost paradoxical fact is also discussed by Low [141]. Therefore, in the far zone, the angular momentum density is

$$\begin{aligned} \mathbf{h}_3^{\text{field far}}(t, r, \vartheta, \varphi; \mathbf{0}) &\approx \frac{d_3^2}{16\pi^2 \epsilon_0 c} r f_1(\delta_3) f_2(\delta_3) \sin \vartheta \cos \vartheta \hat{\boldsymbol{\phi}} \\ &= -\frac{k^3 d_3^2}{64\pi^2 \epsilon_0 r^2 c} \sin[2(kr - \omega t + \delta_3)] \sin 2\vartheta \hat{\boldsymbol{\phi}} \quad (70) \end{aligned}$$

This result shows that $\mathbf{h}_3^{\text{field far}}$ has the expected r^{-2} fall off, has no z component, and oscillates at 2ω along $-\hat{\boldsymbol{\phi}}$. This causes an electric charge in the far zone but not located at $\vartheta = n\pi/2, n \in \mathbb{Z}$ to rotate around its own center of mass in the osculating plane normal to $\hat{\boldsymbol{\phi}}$. However, the temporal (cycle) average of $\mathbf{h}_3^{\text{field far}}$ is zero, which makes it nontrivial to measure this rotational motion. It is tempting to relate this and similar double-frequency terms to Zitterbewegung [35].

b. Two co-located crossed Hertzian dipoles We now want to calculate the field linear and angular momenta emitted from a system of two co-located monochromatic Hertzian dipoles, one spatially rotated from the other by $\pi/2$, fed at the same frequency but with different temporal phase shifts. For this purpose we chose the two Hertzian dipoles $\mathbf{d}_j, j = 1, 2$ with their generated fields described by Eqns. (B14). Since the total field is a superposition of the fields from the two individual dipoles, the total linear momentum density $\mathbf{g}_{1\&2}^{\text{field}}$ emitted by the two dipoles is

$$\begin{aligned} \mathbf{g}_{1\&2}^{\text{field}} &= \epsilon_0 (\mathbf{E}_1 + \mathbf{E}_2) \times (\mathbf{B}_1 + \mathbf{B}_2) \\ &= \epsilon_0 \mathbf{E}_1 \times \mathbf{B}_1 + \epsilon_0 \mathbf{E}_2 \times \mathbf{B}_2 + \epsilon_0 \mathbf{E}_1 \times \mathbf{B}_2 + \epsilon_0 \mathbf{E}_2 \times \mathbf{B}_1 \\ &= \mathbf{g}_1^{\text{field}} + \mathbf{g}_2^{\text{field}} + \mathbf{g}_{12}^{\text{field}} + \mathbf{g}_{21}^{\text{field}} \quad (71) \end{aligned}$$

We see that in addition to the vector sum of the two linear momentum densities from the individual dipoles \mathbf{d}_1 and \mathbf{d}_2 , the total linear momentum contains two interference terms $\mathbf{g}_{12}^{\text{field}}$ and $\mathbf{g}_{21}^{\text{field}}$ which appear due to the fact that the total electromagnetic field is the superposition of the fields from each dipole. Using Eqns. (B15)–(B16) and (B18)–(B19), we can calculate the exact expression for $\mathbf{g}_{1\&2}^{\text{field}}$, and from that, using Eqn. (A37), the exact expression for the total angular momentum density $\mathbf{h}_{1\&2}^{\text{field}}$. If the two dipole moments have equal

amplitudes, $d_1 = d_2 = d$, and are in phase quadrature relative each other, $\delta_1 = 0$ and $\delta_2 = \pi/2$, we find that the exact expression for the z component of the angular momentum density $\mathbf{h}_{1\&2}^{\text{field}}$, valid in all of space outside the dipoles, is

$$\begin{aligned} h_{1\&2z}^{\text{field}}(t, r, \vartheta, \varphi; \mathbf{0}) &= \frac{d^2(\mathbf{0})k}{8\pi^2 \epsilon_0 c} \left(\frac{k^2}{r^2} \{ \sin^2 \varphi \cos^2(kr - \omega t) \right. \\ &\quad + \cos^2 \varphi \sin^2(kr - \omega t) + \sin \varphi \cos \varphi \sin[2(kr - \omega t)] \} \\ &\quad + \frac{k}{r^3} \{ 2 \sin \varphi \cos \varphi [\cos^2(kr - \omega t) - \sin^2(kr - \omega t)] \\ &\quad \quad - (\sin^2 \varphi - \cos^2 \varphi) \sin[2(kr - \omega t)] \} \\ &\quad \left. + \frac{1}{r^4} \{ \cos^2 \varphi \cos^2(kr - \omega t) + \sin^2 \varphi \sin^2(kr - \omega t) \right. \\ &\quad \quad \left. - \sin \varphi \cos \varphi \sin[2(kr - \omega t)] \} \right) \sin^2 \vartheta \quad (72) \end{aligned}$$

To turn the z component of the angular momentum density, $h_{1\&2z}^{\text{field}}$, radiated from two co-located Hertzian dipoles, arranged perpendicular to each other and oscillating in quadrature phase, into the observable z component of the total field angular momentum, $J_z^{\text{field}}(\mathbf{0})$, we must integrate (72) over an observation volume V . Choosing V as in Eqn. (65), *i.e.*, as the region between two spherical shells with radii r_0 and $r_0 + \Delta r_0$, representing the radial extent of the ‘‘pulse’’ emitted, we obtain

$$J_{1\&2z}^{\text{field}}(t, \mathbf{0}) = \int_{r_0}^{r_0 + \Delta r_0} dr r^2 \int_{\vartheta_1}^{\vartheta_2} d\vartheta \sin \vartheta \int_{\varphi_1}^{\varphi_2} d\varphi h_{1\&2z}^{\text{field}}(\mathbf{0}) \quad (73)$$

where $h_{1\&2z}^{\text{field}}(\mathbf{0})$ is given by Eqn. (72).

If we integrate over all azimuth angles φ from $\varphi_1 = 0$ to $\varphi_1 = 2\pi$, and also use the well-known identities

$$\int_0^{2\pi} d\varphi \sin^2 \varphi = \int_0^{2\pi} d\varphi \cos^2 \varphi = \pi \quad (74a)$$

$$\int_0^{2\pi} d\varphi \sin \varphi \cos \varphi = 0 \quad (74b)$$

$$\sin^2(kr - \omega t) + \cos^2(kr - \omega t) = 1 \quad (74c)$$

we obtain

$$J_{1\&2z}^{\text{field}}(t, \mathbf{0}) = \frac{d^2(\mathbf{0})k}{8\pi \epsilon_0 c} \int_{r_0}^{r_0 + \Delta r_0} dr \left(k^2 + \frac{1}{r^2} \right) \int_{\vartheta_1}^{\vartheta_2} d\vartheta \sin^3 \vartheta \quad (75)$$

If we now integrate over all polar angles ϑ from $\vartheta_1 = 0$ to $\vartheta_2 = \pi$, we obtain the explicit, closed-form expression

$$J_{1\&2z}^{\text{field}}(t, \mathbf{0}) = \frac{d^2(\mathbf{0})k}{6\pi \epsilon_0 c} \left(k^2 \Delta r_0 + \frac{\Delta r_0}{k^2 r_0 (r_0 + \Delta r_0)} \right) \quad (76)$$

where the only time dependence comes from the duration of the emitted ‘‘pulse’’ $\Delta t = \Delta r_0/c$. When the distance r_0 that the ‘‘pulse’’ has propagated is very large so that the $1/r_0^2$ contribution can be neglected, the z component of the field angular momentum can be approximated by

$$J_{1\&2z}^{\text{field far}}(t, \mathbf{0}) = \frac{d^2(\mathbf{0})k}{6\pi \epsilon_0 c} k^2 \Delta r_0 = \frac{d^2(\mathbf{0})k^3}{6\pi \epsilon_0} \Delta t \quad (77)$$

which propagates without radial fall-off as expected.

If the observation volume V , *i.e.*, the angular momentum sensing antenna, is a very thin circular ring in the xy plane ($\vartheta = \pi/2$) centered on the dipoles and with a radius r_0 , the integrals in Eqn. (73) are trivial and the result is

$$J_{1\&2z}^{\text{field}}(t, \mathbf{0}) = \frac{d^2(\mathbf{0})k}{8\pi\epsilon_0 c} \left(k^2 + \frac{1}{r_0^2} \right) \quad (78)$$

The experimental results in [108] agree with this prediction. Comparing Eqn. (78) with Eqn. (4) in [108], shows that the latter is in error; there is a factor of 2π missing which explains the factor of ~ 6 discrepancy.

3. Special angular momentum antennas

Proof-of-concept experiments have shown that it is possible to use the total angular momentum, *i.e.*, the SAM+OAM physical observable, as a new physical layer for radio science and technology exploitation. These studies include numerical experiments [57] showing that it is feasible to utilize OAM in radio; controlled anechoic chamber laboratory experiments [60] verifying that it is possible to generate and transmit radio beams carrying non-integer OAM and to measure their OAM spectra in the form of weighted superpositions of different integer OAM eigenmodes each with its own quantum number (mode index), also known as topological charge; and outdoor experiments [61, 67, 142], verifying that in a real-world setting different signals, physically encoded in different OAM modes and overlapping each other in space and time, can be transmitted independently to a receiver located in the (linear momentum) far zone and be resolved there. These experimental findings have recently been verified in independent laboratory experiments [67].

Transducers that are capable of generating and detecting angular momentum directly will have to be at least two-dimensional. An example is the flat plate antenna developed by Bennis *et al.* [140]. Alternatively, one can equip single linear-momentum antennas with azimuthally dependent reflectors or lenses [60, 67]. This includes helicoidal parabolic antennas [61, 143].

C. Angular momentum and multi-transducer techniques

The multi-antenna technique for enhancing the capacity of a link using linear momentum that goes by the name multiple-input-multiple-output (MIMO) amounts to utilizing the fact that the EM linear momentum $\mathbf{p}^{\text{field}}$ emitted from an ordinary antenna—typically a linear dipole—is a vector quantity. Dividing this EM linear momentum vector up into M equal components such that

$$\mathbf{p}^{\text{field}} = \sum_{n=1}^M \mathbf{p}_n^{\text{field}} \quad (79)$$

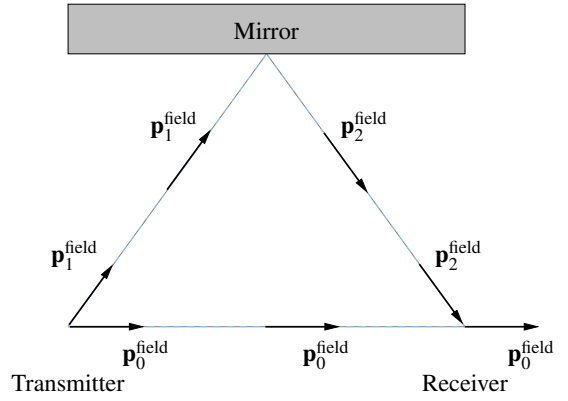


Figure 5. Communicating with electromagnetic linear momentum $\mathbf{p}^{\text{field}}$ in the presence of a reflective surface. In the two-dimensional plane of the figure, the vector $\mathbf{p}_0^{\text{field}}$ propagates directly along the straight path to the receiver, while the vector $\mathbf{p}_1^{\text{field}}$ is reflected off the mirror without recoil and produces the vector $\mathbf{p}_2^{\text{field}}$ at the receiver. Since $\mathbf{p}^{\text{field}}$ is a constant of the motion and preserves its parity upon reflection, the full 3D structure of the EM linear momentum can be obtained by post-processing. This is used in present MIMO schemes for enhancing the spectral density of linear-momentum radio communications in reflective environments.

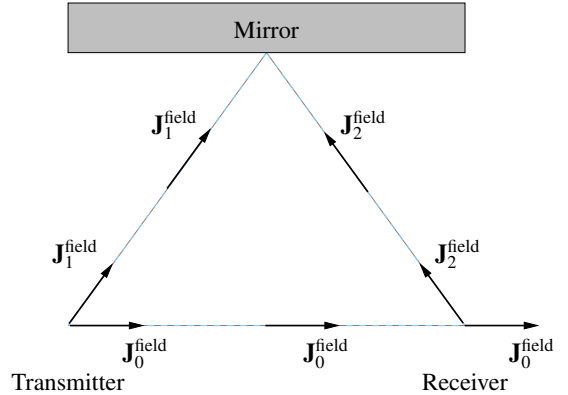


Figure 6. Communicating with electromagnetic angular momentum $\mathbf{J}^{\text{field}}$ in the presence of a reflecting surface. Angular momentum is a pseudovector and therefore $\mathbf{J}^{\text{field}}$ suffers a parity change when it is reflected off a dense medium. Taking this parity change into account properly, the reflected pseudovector can be used in MIMO-type schemes for enhancing the spectral density of angular-momentum radio communications, over and above the enhancement offered by the multi-state capability of angular momentum relative to the single-state linear momentum.

letting each $\mathbf{p}_n^{\text{field}}$ be emitted from one of M linear momentum antennas and propagate along different paths to the receiving end where the individual EM linear momenta $\mathbf{p}_n^{\text{field}}$ are combined vectorially, the spectral efficiency and/or the signal-to-noise-ratio (SNR) can, under certain circumstances be increased.

A MIMO-like enhancement of the radio spectral capacity can be achieved by the alternative technique of letting a beam of linear momentum $\mathbf{p}^{\text{field}}$ emitted from an antenna be reflected off a wall, say. This works because the linear momentum

Table II. Similarities and differences between the EM linear momentum density, $\mathbf{g}^{\text{field}}(t, \mathbf{x})$, and the EM angular momentum density around a moment point \mathbf{x}_0 , $\mathbf{h}^{\text{field}}(t, \mathbf{x}, \mathbf{x}_0)$, carried by a classical electromagnetic field $[\mathbf{E}(t, \mathbf{x}), \mathbf{B}(t, \mathbf{x})]$ in the presence of matter (particles) with mechanical linear momentum density $\mathbf{g}^{\text{mech}}(t, \mathbf{x})$ and mechanical angular momentum density $\mathbf{h}^{\text{mech}}(t, \mathbf{x}, \mathbf{x}_0)$.

Property	Linear momentum density	Angular momentum density
Definition	$\mathbf{g}^{\text{field}} = \epsilon_0 \mathbf{E} \times \mathbf{B}$	$\mathbf{h}^{\text{field}} = (\mathbf{x} - \mathbf{x}_0) \times (\epsilon_0 \mathbf{E} \times \mathbf{B})$
SI unit	N s m^{-3} ($\text{kg m}^{-2} \text{s}^{-1}$)	N s m^{-2} ($\text{kg m}^{-1} \text{s}^{-1}$)
Spatial fall off at large distances r	$\sim r^{-2} + \mathcal{O}(r^{-3})$	$\sim r^{-2} + \mathcal{O}(r^{-3})$
Typical phase factor	$\exp\{i(kz - \omega t)\}$	$\exp\{i(\alpha\varphi + kz - \omega t)\}$
C (charge conjugation) symmetry	Even	Even
P (spatial inversion) symmetry	Even (polar vector, ordinary vector)	Odd (axial vector, pseudovector)
T (time reversal) symmetry	Odd	Odd

density (Poynting) vector is an ordinary (polar) vector and therefore does not suffer any parity change upon reflection. This is illustrated schematically in Fig. 5; see also Fig. 1 in Andrews *et al.* [144] where the authors plot a vector that they call “polarization,” which apparently is the (approximate) far-field electric field vector.

For this to work, the Heisenberg uncertainty relation for momentum must be fulfilled. If λ denotes the wavelength, then $p_n^{\text{field}} = \hbar/\lambda$ is the x component of the linear momentum of each photon of the monochromatic radio beam emitted from the n th antenna and this relation becomes

$$\Delta p_n^{\text{field}} \Delta x \geq \hbar/2$$

Hence the spatial separation Δx between the linear momenta must be at least $\lambda/2$ in order to be statistically independent. In practical radio implementations this means that the distance between one (translational current carrying) antenna and another one must fulfill the inequality

$$\Delta x \geq \lambda/2$$

Consequently, the space-time distance between each individual linear-momentum MIMO antenna must be at least half a wavelength; in practical implementations the separation must be much larger. This limits the usefulness of the MIMO technique in practice. Furthermore, MIMO often requires substantial post-processing and this limits its usefulness even further [83, 145, 146].

As described earlier, when wireless communication is based on the angular momentum physics layer, it is possible, in an ideal case, to N -tuple the capacity within a fixed frequency bandwidth of a SISO system using single monolithic antennas at both the transmitting and the receiving ends. Furthermore, replacing the single antennas by M transmitting and receiving antennas to split the orbital angular momentum (OAM) pseudovector into M equal units $\mathbf{L}_n^{\text{field}}$

$$\mathbf{L}^{\text{field}} = \sum_{n=1}^M \mathbf{L}_n^{\text{field}} \quad (80)$$

it should be possible to achieve an $N \times M$ -fold increase in capacity. Using, in addition to this OAM MIMO technique, also wave polarization (spin angular momentum, SAM), the total capacity will be $2N \times M$ higher than for a linear-momentum

SISO channel. As illustrated in Figure 6, the exploitation of the angular momentum technique in a reflective environment requires that the parity of $\mathbf{J}^{\text{field}}$ can be taken properly into account. Experiments have shown that this is feasible [147].

V. SUMMARY

We have presented a review of those fundamental physical principles that comprise the foundation for radio science and technology. We have clarified that in electromagnetic experiments and applications such as wireless communications, one has to rely on the existence and judicious use of electromagnetic observables and have emphasized the fact that by exploiting the angular momentum observable, in addition to the linear momentum observable, many advantages can be achieved.

The similarities and differences between linear momentum and angular momentum based techniques in radio science and communication applications are summarized in Table II and in the following list:

1. Techniques based on the linear momentum degrees of freedom of an electromechanical system exploits the translational degrees of freedom of the EM field and the associated particles.
 - (a) The linear momentum $\mathbf{p}^{\text{field}}(t)$ can be measured remotely—and thereby utilized in applications—by using a conduction current based device that integrates the local linear momentum density $\mathbf{g}^{\text{field}}(t, \mathbf{x})$ over a one-dimensional volume V , typically a very thin cylinder as is the case for a linear electric dipole antenna. From such a nonlocal measurement one can estimate the (weighted) average of the primary EM field over V but not determine the exact field (within instrumental errors).
2. Techniques based on the angular momentum degrees of freedom of an electromechanical system exploits the rotational degrees of freedom of the EM field and the associated particles.

- (a) The angular momentum $\mathbf{J}^{\text{field}}(t)$ can be measured remotely—and thereby utilized in applications—by using a conduction current based device, or a spin- and/or orbit current based device, that integrates the local angular momentum density $\mathbf{h}^{\text{field}}(t, \mathbf{x})$ over a two- or three-dimensional volume.
- (b) In a beam situation typical for radio communication links, radio astronomy observations, and radar applications, the spin and angular parts of the angular momentum, Σ^{field} and $\mathbf{J}^{\text{field}}$ respectively, can be separated (or, alternatively, both the helicity and the total angular momentum of the beam can be measured). The main differences between the two parts of the angular momenta are:
- i. The spin part of the angular momentum (SAM, polarization), Σ^{field} , manifests itself as a rotation in time of the field vectors such that they have different directions (oscillation phase) modulo 2π at one position \mathbf{x} in the phase front at different times t and $t + \Delta t$. Hence, the measurement of SAM (polarization) requires temporal coherence.
 - ii. The orbital part of the angular momentum (OAM, twist), $\mathbf{L}^{\text{field}}$, manifests itself as a rotation in space of the field vectors such that they have different directions (oscillation phase) modulo 2π at different azimuthal angles φ and $\varphi + \Delta\varphi$ in the phase plane at a given instant t . Hence, the measurement of OAM (twist) requires spatial coherence.

ACKNOWLEDGMENTS

The authors gratefully acknowledge useful discussions with Iwo Białynicki-Birula and Anton Zeilinger. We also thank Göran Fäldt for reminding us about the excellent treatment by Truesdell [86] on the fundamental properties of angular momentum and Olle Eriksson for comments.

B. T. was financially supported by the Swedish National Space Board (SNSB) and the Swedish Research Council (VR) under the contract number 2012-3297. H. T. acknowledges support from EPSRC grant EP/H005188/1 and, for the early stage of the work, from the Centre for Dynamical Processes and Structure Formation, Uppsala University, Sweden.

Appendix A: The ten Poincaré invariants and the corresponding equations of continuity

For completeness, we shall in this Appendix discuss the ten conserved electromagnetic observables that correspond to the ten-dimensional Poincaré symmetry group $P(10)$, *i.e.*, the ten Poincaré invariants and their associated equations of continuity. They are the scalar quantity energy, the three components of the linear momentum vector, the three components of the angular

momentum pseudovector, and the three components of the energy center position vector. Only a small subset of these observables are currently used in radio science, optics, and wireless communications.

All in all the electromagnetic field has 84 constants of motion [148]. If all conserved quantities of an integrable physical system are known, the system dynamics can be obtained trivially by formulating it in terms of action-angle variables. Electromagnetic conservation laws can be viewed as constraints on the field dynamics and, in this sense, every conserved quantity is physically significant. The information contained in the conserved quantities corresponds one-to-one to the information contained in the Maxwell-Lorentz postulates [149].

1. Energy

The energy density $u^{\text{field}}(t, \mathbf{x})$ carried by the fields generated by the sources in V' is

$$u^{\text{field}} = \frac{\epsilon_0}{2} (\mathbf{E} \cdot \mathbf{E} + c^2 \mathbf{B} \cdot \mathbf{B}) \quad (\text{A1a})$$

which, according to Eqns. (2) and Table I, can be written

$$u^{\text{field}} = \frac{\epsilon_0}{2} \mathbf{G} \cdot \mathbf{G}^* = \frac{\epsilon_0}{2} |\mathbf{G}|^2 = \frac{\epsilon_0}{2} \sqrt{(\mathbf{G} \cdot \mathbf{G})(\mathbf{G} \cdot \mathbf{G})^*} \quad (\text{A1b})$$

Outside the source volume, the field energy in a certain observation volume V can be measured with an appropriate energy sensor, *e.g.*, a calorimeter or bolometer, that integrates u^{field} over V .

With the energy flux vector (Poynting vector) $\mathbf{S}(t, \mathbf{x})$ given by the formula

$$\mathbf{S} = \epsilon_0 c^2 \mathbf{E} \times \mathbf{B} \quad (\text{A2a})$$

or, using Eqns. (2) and Table I,

$$\mathbf{S} = i \frac{\epsilon_0 c}{2} \mathbf{G} \times \mathbf{G}^* \quad (\text{A2b})$$

the energy density balance equation, which follows straightforwardly from the Maxwell-Lorentz equations (1), takes the form

$$\frac{\partial u^{\text{field}}}{\partial t} + \nabla \cdot \mathbf{S} = -\mathbf{j}^e \cdot \mathbf{E} \quad (\text{A3})$$

i.e., a local continuity equation for the field energy density with a sink (loss) term $\mathbf{j}^e \cdot \mathbf{E}$. By using Eqns. (2), (A1b), and (A2b), we can write this as

$$\frac{\partial (\mathbf{G} \cdot \mathbf{G}^*)}{\partial t} + ic \nabla \cdot (\mathbf{G} \times \mathbf{G}^*) = -\frac{1}{\epsilon_0} \mathbf{j}^e \cdot (\mathbf{G} + \mathbf{G}^*) \quad (\text{A4})$$

If $\rho^{\text{mech}}(t', \mathbf{x}')$ denotes the local mechanical mass density field and $\mathbf{v}^{\text{mech}}(t', \mathbf{x}')$ the local mechanical velocity field of the charged particles at a point in V' , then, in the approximation where statistical mechanics as well as relativistic and

quantum physics effects are negligible, the electric current density $\mathbf{j}^e(t', \mathbf{x}')$ carried by the charged particles can be written as $\mathbf{j}^e = \rho^e \mathbf{v}^{\text{mech}}$ and the loss term in Eqn. (A3) can therefore be identified as the increase in mechanical energy density of the particles [3, 4]:

$$\frac{\partial u^{\text{mech}}}{\partial t} = \mathbf{j}^e \cdot \mathbf{E} = \mathbf{v}^{\text{mech}} \cdot \rho^e \mathbf{E} \quad (\text{A5})$$

representing dissipation due to Ohmic losses, *i.e.*, transfer of field energy density to mechanical energy density of the current-carrying particles.

This identification makes it possible to introduce the total energy density of the electromechanical system under study (charged particles and their associated fields)

$$u^{\text{sys}}(t, \mathbf{x}) = u^{\text{field}}(t, \mathbf{x}) + u^{\text{mech}}(t, \mathbf{x}) \quad (\text{A6})$$

and to put Eqn. (A3) in the form of an equation of continuity where there are no sources or sinks (losses) [3, 4]:

$$\frac{\partial u^{\text{sys}}}{\partial t} + \nabla \cdot \mathbf{S} = 0 \quad (\text{A7})$$

We let $U(t)$ denote energy (volume integrated energy density). Then, in obvious notation, the system energy is the sum of the energy of the particles and the energy of the field:

$$U^{\text{sys}}(t) = \int_V d^3x u^{\text{sys}}(t, \mathbf{x}) = U^{\text{field}}(t) + U^{\text{mech}}(t) \quad (\text{A8})$$

Volume integrating the local continuity equation (A7) and using the divergence theorem, the corresponding global continuity equation can be written

$$\frac{dU^{\text{sys}}}{dt} + \oint_S d^2x \hat{\mathbf{n}} \cdot \mathbf{S} = 0 \quad (\text{A9})$$

This is the Poynting theorem, also known as the energy theorem in Maxwell's theory. It is utilized, for instance, in radiometry. The field energy itself is utilized in simple, broadband "on-off" signaling as was used in Marconi's first radio experiments and also in optical fiber communications. The conservation of energy as described by (A9) is a manifestation of the temporal translation invariance symmetry of electrodynamics and describes the kinematics of the system.

2. Linear momentum

The electromagnetic linear momentum density $\mathbf{g}^{\text{field}}(t, \mathbf{x})$ radiated from V' is [3–5, 53]

$$\mathbf{g}^{\text{field}} = \epsilon_0 \mathbf{E} \times \mathbf{B} \quad (\text{A10})$$

or, using Eqns. (2),

$$\mathbf{g}^{\text{field}} = i \frac{\epsilon_0}{2c} \mathbf{G} \times \mathbf{G}^* \quad (\text{A11})$$

and is, in free space, simply related to the Poynting vector (A2) by the Planck relation

$$\mathbf{S} = c^2 \mathbf{g}^{\text{field}} \quad (\text{A12})$$

Let us introduce the electromagnetic linear momentum flux tensor $\mathbf{T}(t, \mathbf{x})$ as the negative of Maxwell's stress tensor [3, 5]

$$\mathbf{T} = u^{\text{field}} \mathbb{1}_3 - \epsilon_0 (\mathbf{E} \otimes \mathbf{E} + c^2 \mathbf{B} \otimes \mathbf{B}) \quad (\text{A13a})$$

or, using Eqns. (2),

$$\mathbf{T} = \frac{\epsilon_0}{2} [\mathbf{G} \cdot \mathbf{G}^* \mathbb{1}_3 - (\mathbf{G} \otimes \mathbf{G}^* + \mathbf{G}^* \otimes \mathbf{G})] \quad (\text{A13b})$$

where $\mathbb{1}_3$ is the rank-3 unit tensor and \otimes the tensor (Kronecker, dyadic) product operator. Then the balance equation for linear momentum density that follows from the Maxwell-Lorentz equations (1) can be written [3–5]

$$\frac{\partial \mathbf{g}^{\text{field}}}{\partial t} + \nabla \cdot \mathbf{T} = -\mathbf{f} \quad (\text{A14a})$$

where

$$\mathbf{f}(t, \mathbf{x}) = \rho^e(t, \mathbf{x}) \mathbf{E}(t, \mathbf{x}) + \mathbf{j}^e \times \mathbf{B}(t, \mathbf{x}) \quad (\text{A14b})$$

This polar vector \mathbf{f} is the Lorentz force density[150] that behaves like a loss of field linear momentum density.

By using Eqns. (2), (A11), and (A13b) we can write this local equation of continuity for linear momentum density as

$$\begin{aligned} \frac{\partial (\mathbf{G} \times \mathbf{G}^*)}{\partial t} - ic \nabla \cdot (\mathbf{G} \cdot \mathbf{G}^* \mathbb{1}_3 - \frac{1}{\epsilon_0} (\mathbf{G} \otimes \mathbf{G}^* + \mathbf{G}^* \otimes \mathbf{G})) \\ = -i \frac{c}{\epsilon_0} [\rho^e (\mathbf{G} + \mathbf{G}^*) - \epsilon_0 \mathbf{j}^e \times (\mathbf{G} - \mathbf{G}^*)] \end{aligned} \quad (\text{A15})$$

In an electromechanical system of charged, massive particles and pertinent fields, *e.g.*, a transmitting antenna, the mechanical linear momentum density the particles is

$$\mathbf{g}^{\text{mech}}(t, \mathbf{x}) = \rho^{\text{mech}}(t, \mathbf{x}) \mathbf{v}^{\text{mech}}(t, \mathbf{x}) \quad (\text{A16})$$

The local equation of continuity of linear momentum of an electromechanical system, directly derivable from Maxwell's equations, can therefore be written [3–5, 55]

$$\frac{\partial \mathbf{g}^{\text{sys}}}{\partial t} + \nabla \cdot \mathbf{T} = \mathbf{0} \quad (\text{A17})$$

where

$$\mathbf{g}^{\text{sys}}(t, \mathbf{x}) = \mathbf{g}^{\text{field}}(t, \mathbf{x}) + \mathbf{g}^{\text{mech}}(t, \mathbf{x}) \quad (\text{A18})$$

is the system linear momentum density.

The classical electromagnetic field linear momentum $\mathbf{p}^{\text{field}}$ that is localized inside a volume V embedded in free space is obtained by volume integrating the linear momentum density $\mathbf{g}^{\text{field}}$ over V [4, 5, 55]

$$\mathbf{p}^{\text{field}}(t) = \int_V d^3x \mathbf{g}^{\text{field}}(t, \mathbf{x}) = \epsilon_0 \int_V d^3x [\mathbf{E}(t, \mathbf{x}) \times \mathbf{B}(t, \mathbf{x})] \quad (\text{A19})$$

This integration can be done by using an appropriate volume integrating linear momentum sensor, *e.g.*, a linear dipole antenna.

The mechanical linear momentum in V is

$$\mathbf{p}^{\text{mech}}(t) = \int_V d^3x \mathbf{g}^{\text{mech}}(t, \mathbf{x}) = \int_V d^3x \rho^{\text{mech}}(t, \mathbf{x}) \mathbf{v}^{\text{mech}}(t, \mathbf{x}) \quad (\text{A20})$$

which means that the total linear momentum of the system of particles and fields in V is

$$\mathbf{p}^{\text{sys}}(t) = \mathbf{p}^{\text{field}}(t) + \mathbf{p}^{\text{mech}}(t) \quad (\text{A21})$$

It fulfills the global conservation law [3, 4, 6]

$$\frac{d\mathbf{p}^{\text{sys}}}{dt} + \oint_S d^2x \hat{\mathbf{n}} \cdot \mathbf{T} = \mathbf{0} \quad (\text{A22})$$

This is the linear momentum theorem in Maxwell's theory. It demonstrates that not only the mechanical particles (charges) but also the electromagnetic field itself carries linear momentum (translational momentum) that couples to the mechanical linear momentum of the matter (charged particles) and thereby to the conduction current carried by the charged particles.

a. Gauge invariance

It is common practice to investigate the properties of the electromagnetic observables that we consider here, by expressing the fields in terms of their potentials [151]. If the vector potential $\mathbf{A}(t, \mathbf{x})$ is twice continuously differentiable in space, it is well known that it fulfills the vector analytic identity [see, *e.g.*, Thidé [6]]

$$\begin{aligned} \mathbf{A}(t, \mathbf{x}) = & -\nabla \int_{V'} d^3x' \frac{\nabla' \cdot \mathbf{A}(t, \mathbf{x}')}{4\pi|\mathbf{x} - \mathbf{x}'|} \\ & + \nabla \times \int_{V'} d^3x' \frac{\nabla' \times \mathbf{A}(t, \mathbf{x}')}{4\pi|\mathbf{x} - \mathbf{x}'|} \\ & - \oint_{S'} d^2x' \hat{\mathbf{n}}' \cdot \left(\frac{\mathbf{A}(t, \mathbf{x}') \otimes (\mathbf{x} - \mathbf{x}')}{|\mathbf{x} - \mathbf{x}'|^3} \right) \end{aligned} \quad (\text{A23})$$

The last integral, to be evaluated over a surface S' enclosing the entire volume V' within which $\mathbf{A} \neq \mathbf{0}$ is localized, vanishes if it is evaluated at very large distances and the expression within the big parentheses falls off faster than $1/|\mathbf{x} - \mathbf{x}'|^2 = 1/r^2$, or if it is perpendicular to the normal unit vector $\hat{\mathbf{n}}'$, or if it has certain (a)symmetry properties.[152]. Then, Helmholtz's decomposition is applicable, allowing us to write

$$\mathbf{A}(t, \mathbf{x}) = \mathbf{A}^{\text{irrot}}(t, \mathbf{x}) + \mathbf{A}^{\text{rotat}}(t, \mathbf{x}) \quad (\text{A24})$$

where $\mathbf{A}^{\text{irrot}}$ is the irrotational part of \mathbf{A} , fulfilling $\nabla \times \mathbf{A}^{\text{irrot}} = \mathbf{0}$, and $\mathbf{A}^{\text{rotat}}$ is the rotational part, fulfilling $\nabla \cdot \mathbf{A}^{\text{rotat}} = 0$. Hence $\mathbf{A}^{\text{rotat}}$ is gauge invariant by definition, and

$$\mathbf{B}(t, \mathbf{x}) = \nabla \times \mathbf{A}(t, \mathbf{x}) = \nabla \times \mathbf{A}^{\text{rotat}}(t, \mathbf{x}) \quad (\text{A25})$$

If we take (A19) as a starting point, and assume that not only the vector potential \mathbf{A} can be Helmholtz decomposed, but also \mathbf{E} is so well-behaved that it can be decomposed as

$$\mathbf{E}(t, \mathbf{x}) = \mathbf{E}^{\text{irrot}}(t, \mathbf{x}) + \mathbf{E}^{\text{rotat}}(t, \mathbf{x}) \quad (\text{A26})$$

then the electromagnetic linear (translational) momentum can be represented by the gauge invariant expression

$$\begin{aligned} \mathbf{p}^{\text{field}}(t) = & \epsilon_0 \int_V d^3x \mathbf{E}^{\text{irrot}} \times (\nabla \times \mathbf{A}^{\text{rotat}}) \\ & + \epsilon_0 \int_V d^3x \mathbf{E}^{\text{rotat}} \times (\nabla \times \mathbf{A}^{\text{rotat}}) \end{aligned} \quad (\text{A27})$$

Using straightforward vector analysis, we obtain the following result [6]

$$\begin{aligned} \mathbf{p}^{\text{field}}(t) = & \int_V d^3x \rho^e \mathbf{A}^{\text{rotat}} - \epsilon_0 \int_V d^3x \mathbf{A}^{\text{rotat}} \times (\nabla \times \mathbf{E}^{\text{rotat}}) \\ & - \epsilon_0 \oint_S d^2x \hat{\mathbf{n}} \cdot \mathbf{E}^{\text{rotat}} \otimes \mathbf{A}^{\text{rotat}} \end{aligned} \quad (\text{A28})$$

Whenever Eqns. (A24) and (A26) hold, this gauge invariant expression for $\mathbf{p}^{\text{field}}$ is exact. If the electric field is such that it cannot be Helmholtz decomposed, every occurrence of $\mathbf{E}^{\text{irrot}}$ and $\mathbf{E}^{\text{rotat}}$ in Eqn. A27 and Eqn. A28 has to be replaced by \mathbf{E} but would still be exact and gauge independent.

If the expression within the big parentheses in the integrand of the last integral in Eqn. (A23) is such that this surface integral grows without bounds at very large distances, it is not possible to decompose the vector potential as described by Eqn. (A24) and $\mathbf{A}^{\text{rotat}}$ and $\mathbf{E}^{\text{rotat}}$ in Eqn. A27 and Eqn. A28 would have to be replaced by \mathbf{A} and \mathbf{E} .

b. First quantization formalism

If we restrict ourselves to consider a single temporal Fourier component of the rotational ('transverse') component of \mathbf{E} in a region where $\rho^e = 0$, we find that in complex representation

$$\mathbf{E}^{\text{rotat}} = -\frac{\partial \mathbf{A}^{\text{rotat}}}{\partial t} = i\omega \mathbf{A}^{\text{rotat}} \quad (\text{A29})$$

which allows us to replace $\mathbf{A}^{\text{rotat}}$ by $-i\mathbf{E}^{\text{rotat}}/\omega$, yielding,

$$\begin{aligned} \langle \mathbf{p}^{\text{field}} \rangle_t = & \text{Re} \left\{ -i \frac{\epsilon_0}{2\omega} \int_V d^3x (\nabla \otimes \mathbf{E}^{\text{rotat}}) \cdot (\mathbf{E}^{\text{rotat}})^* \right\} \\ & + \text{Re} \left\{ i \frac{\epsilon_0}{2\omega} \oint_S d^2x \hat{\mathbf{n}} \cdot \mathbf{E}^{\text{rotat}} \otimes (\mathbf{E}^{\text{rotat}})^* \right\} \end{aligned} \quad (\text{A30})$$

If the tensor (dyadic) $\mathbf{E} \otimes (\mathbf{E}^{\text{rotat}})^*$ is regular and falls off sufficiently rapidly at large distances or if $\hat{\mathbf{n}} \cdot \mathbf{E} = 0$, we can discard the surface integral term and find that the cycle averaged linear momentum carried by the rotational components of the fields, $\mathbf{E}^{\text{rotat}}$ and $\mathbf{B}^{\text{rotat}} \equiv \mathbf{B} = \nabla \times \mathbf{A}^{\text{rotat}}$, is

$$\langle \mathbf{p}^{\text{field}} \rangle_t = \text{Re} \left\{ -i \frac{\epsilon_0}{2\omega} \int_V d^3x (\nabla \otimes \mathbf{E}^{\text{rotat}}) \cdot (\mathbf{E}^{\text{rotat}})^* \right\} \quad (\text{A31})$$

In complex tensor notation this can be written

$$\begin{aligned}\langle \mathbf{p}^{\text{field}} \rangle_t &= -i \frac{\epsilon_0}{2\omega} \sum_{i,j=1}^3 \int_V d^3x (E_i^{\text{rotat}})^* (\hat{\mathbf{x}}_j \partial_j E_i^{\text{rotat}}) \\ &= -i \frac{\epsilon_0}{2\omega} \sum_{i=1}^3 \int_V d^3x (E_i^{\text{rotat}})^* \nabla E_i^{\text{rotat}}\end{aligned}\quad (\text{A32})$$

Making use of the field linear momentum operator, Eqn. (5), we can write the expression for the linear momentum of the electromagnetic field in terms of this operator as

$$\langle \mathbf{p}^{\text{field}} \rangle_t = \frac{\epsilon_0}{2\hbar\omega} \sum_{i=1}^3 \int_V d^3x (E_i^{\text{rotat}})^* \hat{\mathbf{p}}^{\text{field}} E_i^{\text{rotat}} \quad (\text{A33})$$

If we introduce the vector

$$\Psi = \sum_{i=1}^3 \Psi_i \hat{\mathbf{x}}_i = \sqrt{\frac{\epsilon_0}{2\hbar\omega}} \mathbf{E}^{\text{rotat}} = \sqrt{\frac{\epsilon_0}{2\hbar\omega}} \sum_{i=1}^3 E_i^{\text{rotat}} \hat{\mathbf{x}}_i \quad (\text{A34})$$

we can write

$$\langle \mathbf{p}^{\text{field}} \rangle_t = \sum_{i=1}^3 \int_V d^3x \Psi_i^* \hat{\mathbf{p}}^{\text{field}} \Psi_i \quad (\text{A35})$$

or, if we assume Einstein's summation convention,

$$\langle \mathbf{p}^{\text{field}} \rangle_t = \langle \Psi_i | \hat{\mathbf{p}}^{\text{field}} | \Psi_i \rangle \quad (\text{A36})$$

Thus we can represent the cycle (temporal) averaged linear momentum carried by a monochromatic electromagnetic field as a sum of diagonal quantal matrix elements (expectation values) where the rotational ('transverse') component of the (scaled) electric field vector behaves as a kind of vector wavefunction.

Methods based on electromagnetic linear momentum are used for radio science and radar applications, and for wireless communications.

3. Angular momentum

The volumetric density of the electromagnetic field angular momentum, radiated from V' is [53, Sect. 10.6], [3, 6]

$$\mathbf{h}^{\text{field}}(t, \mathbf{x}; \mathbf{y}) = (\mathbf{x} - \mathbf{y}) \times \mathbf{g}^{\text{field}} = \epsilon_0 (\mathbf{x} - \mathbf{y}) \times (\mathbf{E} \times \mathbf{B}) \quad (\text{A37})$$

where $\mathbf{y} = \sum_{j=1}^3 y_j \hat{\mathbf{x}}_j$ is a regular but otherwise arbitrary point (the moment point). Using Eqns. (2), we can write this in complex notation as

$$\mathbf{h}^{\text{field}}(t, \mathbf{x}; \mathbf{y}) = i \frac{\epsilon_0}{2c} (\mathbf{x} - \mathbf{y}) \times (\mathbf{G} \times \mathbf{G}^*) \quad (\text{A38})$$

The mechanical angular momentum density of the charged particles around \mathbf{y} is

$$\begin{aligned}\mathbf{h}^{\text{mech}}(t, \mathbf{x}; \mathbf{y}) &= (\mathbf{x} - \mathbf{y}) \times \mathbf{g}^{\text{mech}}(t, \mathbf{x}) \\ &= (\mathbf{x} - \mathbf{y}) \times \rho^{\text{mech}}(t, \mathbf{x}) \mathbf{v}^{\text{mech}}(t, \mathbf{x})\end{aligned}\quad (\text{A39})$$

As emphasized by Truesdell [86],[153] angular momentum (also known as moment of momentum) is a physical observable in its own right, in general independent of and not derivable from linear momentum. Therefore, as is well known, the knowledge of one of these two observables does not automatically imply a knowledge of the other. This also follows from Noether's theorem [154, 155].

Let us introduce the electromagnetic angular momentum flux pseudotensor

$$\mathbf{M}(\mathbf{y}) = (\mathbf{x} - \mathbf{y}) \times \mathbf{T} \quad (\text{A40})$$

where \mathbf{T} is defined by formula (A13), and the physically observable the Lorentz torque density pseudovector (axial vector) around the moment point \mathbf{y} is

$$\boldsymbol{\tau}(t, \mathbf{x} - \mathbf{y}) = (\mathbf{x} - \mathbf{y}) \times \mathbf{f}(t, \mathbf{x}) \quad (\text{A41})$$

where \mathbf{f} is the Lorentz force density defined by formula (A14b). Then the following local conservation law can be derived from Maxwell's equations [3, 4, 6]

$$\frac{\partial \mathbf{h}^{\text{field}}(\mathbf{y})}{\partial t} + \nabla \cdot \mathbf{M}(\mathbf{y}) = -\boldsymbol{\tau} \quad (\text{A42})$$

Hence, there is a loss of field angular momentum density to the mechanical angular momentum density, in the form of Lorentz torque density $\boldsymbol{\tau}$, showing that the angular momentum of the electromagnetic field and the rotational dynamics of the charges and currents are coupled to each other.

By using Eqns. (2), (A38), and (A13b) we can write this local equation of continuity for angular momentum density as

$$\begin{aligned}&\frac{\partial [(\mathbf{x} - \mathbf{y}) \times (\mathbf{G} \times \mathbf{G}^*)]}{\partial t} \\ &- i c \nabla \cdot \left[(\mathbf{x} - \mathbf{y}) \times \left(\mathbf{G} \cdot \mathbf{G}^* \mathbf{1}_3 - \frac{1}{\epsilon_0} (\mathbf{G} \otimes \mathbf{G}^* + \mathbf{G}^* \otimes \mathbf{G}) \right) \right] \\ &= -i \frac{c}{\epsilon_0} (\mathbf{x} - \mathbf{y}) \times [\rho^e (\mathbf{G} + \mathbf{G}^*) - \epsilon_0 \mathbf{j}^e \times (\mathbf{G} - \mathbf{G}^*)]\end{aligned}\quad (\text{A43})$$

Recalling the definition (A39) of the mechanical angular momentum density, and that the angular momentum density of the system is

$$\mathbf{h}^{\text{sys}}(t, \mathbf{x}; \mathbf{y}) = \mathbf{h}^{\text{field}}(t, \mathbf{x}; \mathbf{y}) + \mathbf{h}^{\text{mech}}(t, \mathbf{x}; \mathbf{y}) \quad (\text{A44})$$

the continuity equation (A42) can be written

$$\frac{\partial \mathbf{h}^{\text{sys}}(t, \mathbf{x}; \mathbf{y})}{\partial t} + \nabla \cdot \mathbf{M}(\mathbf{y}) = \mathbf{0} \quad (\text{A45})$$

This shows that a volume containing an arbitrary distribution of charge density $\rho^e(t', \mathbf{x}')$ and current density $\mathbf{j}^e(t', \mathbf{x}')$ does not only radiate linear momentum density (Poynting vector) but also angular momentum density into the surrounding free space; see also [121]. However, since angular momentum describes rotations, it cannot be sensed by a single linear dipole or similar one-dimensional linear-momentum sensing antenna.

The total classical electromagnetic angular momentum around an arbitrary moment point \mathbf{y} carried by the electromagnetic field in a volume V is [see also Mandel and Wolf

[53]]

$$\begin{aligned}
\mathbf{J}^{\text{field}}(t; \mathbf{y}) &= \int_V d^3x \mathbf{h}^{\text{field}}(t, \mathbf{x}; \mathbf{y}) \\
&= \epsilon_0 \int_V d^3x \mathbf{x} \times [\mathbf{E}(t, \mathbf{x}) \times \mathbf{B}(t, \mathbf{x})] \\
&\quad - \mathbf{y} \times \epsilon_0 \int_V d^3x [\mathbf{E}(t, \mathbf{x}) \times \mathbf{B}(t, \mathbf{x})] \\
&= \mathbf{J}^{\text{field}}(t; \mathbf{0}) - \mathbf{y} \times \mathbf{p}^{\text{field}}(t)
\end{aligned} \tag{A46}$$

where, in the last step, Eqn. (A19) was used.

The mechanical angular momentum in V is

$$\begin{aligned}
\mathbf{J}^{\text{mech}}(t; \mathbf{y}) &= \int_V d^3x \mathbf{h}^{\text{mech}}(t, \mathbf{x}; \mathbf{y}) \\
&= \int_V d^3x (\mathbf{x} - \mathbf{y}) \times \rho^{\text{mech}}(t, \mathbf{x}) \mathbf{v}^{\text{mech}}(t, \mathbf{x}) \\
&= \mathbf{J}^{\text{mech}}(t; \mathbf{0}) - \mathbf{y} \times \mathbf{p}^{\text{mech}}(t)
\end{aligned} \tag{A47}$$

where, in the last step, Eqn. (A20) was used.

Hence, the total angular momentum of the system of particles and fields in V is

$$\begin{aligned}
\mathbf{J}^{\text{sys}}(t; \mathbf{y}) &= \mathbf{J}^{\text{field}}(t; \mathbf{y}) + \mathbf{J}^{\text{mech}}(t; \mathbf{y}) \\
&= \mathbf{J}^{\text{sys}}(t; \mathbf{0}) - \mathbf{y} \times \mathbf{p}^{\text{sys}}(t)
\end{aligned} \tag{A48}$$

Clearly, if $\mathbf{p}^{\text{sys}} \neq \mathbf{0}$, then it is always possible to find a moment point \mathbf{y} that makes the total system angular momentum vanish. If, on the other hand, $\mathbf{p}^{\text{sys}} = \mathbf{0}$, then the total system angular momentum is independent of moment point \mathbf{y} .

The total angular momentum of the system of charges, currents and fields fulfills the global conservation law [3, 5, 55]

$$\frac{d\mathbf{J}^{\text{sys}}(\mathbf{y})}{dt} + \oint_S d^2x \hat{\mathbf{n}} \cdot \mathbf{M}(\mathbf{y}) = \mathbf{0} \tag{A49}$$

i.e., a continuity equation without sources and sinks showing that for a constant angular momentum flux (including zero) the system's angular momentum is a constant of motion. This is the angular momentum theorem in Maxwell's theory. It shows that not only the mechanical particles (charges) but also the electromagnetic field itself carries angular momentum (rotational momentum) that couples to the mechanical angular momentum of the matter (charged particles) and thereby to the conduction current carried by the charged particles.

We see that the conservation law (A49) describes the angular momentum analogs of the linear momentum processes described by the conservation law (A22) and shows that the use of single monolithic antenna devices based on torque action will allow an alternative way of transferring information but with the added benefit of higher information density offered by the inherent quantized multi-state property of the classical electromagnetic angular momentum.

a. Gauge invariance

If the vector potential can be decomposed as in Subsect. A 2 a and if one used several vector analytic identities

and employing partial integration, it is possible to derive an exact, manifestly gauge invariant expression for the total field angular momentum $\mathbf{J}^{\text{field}}$ that is the sum of two pseudovectors, one independent and one dependent of the moment point \mathbf{y} . The result is [6]

$$\mathbf{J}^{\text{field}}(t, \mathbf{y}) = \boldsymbol{\Sigma}^{\text{field}}(t) + \mathbf{L}^{\text{field}}(t, \mathbf{y}) \tag{A50}$$

where

$$\boldsymbol{\Sigma}^{\text{field}}(t) = \epsilon_0 \int_V d^3x \mathbf{E}(t, \mathbf{x}) \times \mathbf{A}^{\text{rotat}}(t, \mathbf{x}) \tag{A51a}$$

and

$$\begin{aligned}
\mathbf{L}^{\text{field}}(t, \mathbf{y}) &= \int_V d^3x (\mathbf{x} - \mathbf{y}) \times \rho^e(t, \mathbf{x}) \mathbf{A}^{\text{rotat}}(t, \mathbf{x}) \\
&\quad + \epsilon_0 \int_V d^3x (\mathbf{x} - \mathbf{y}) \times ([\nabla \otimes \mathbf{A}^{\text{rotat}}(t, \mathbf{x})] \cdot \mathbf{E}(t, \mathbf{x})) \\
&\quad - \epsilon_0 \oint_S d^2x \hat{\mathbf{n}} \cdot [\mathbf{E}(t, \mathbf{x}) \otimes (\mathbf{x} - \mathbf{y}) \times \mathbf{A}^{\text{rotat}}(t, \mathbf{x})]
\end{aligned} \tag{A51b}$$

The last integral vanishes if the integrand is regular and falls off sufficiently rapidly, becomes perpendicular to $\hat{\mathbf{n}}$, or otherwise causes the surface integral to go to zero at very large distances. However, if the vector potential \mathbf{A} is not regular and/or does not fall off faster than $1/r$ as r tends to infinity, the separation of $\mathbf{J}^{\text{field}}$ into $\boldsymbol{\Sigma}^{\text{field}}$ and $\mathbf{L}^{\text{field}}$ is not gauge invariant and, hence, not unique; *cf.* Leader [156] and Białynicki-Birula and Białynicka-Birula [157].

b. First quantization formalism

Let us now assume that \mathbf{A} is so well-behaved that the conditions for Helmholtz's decomposition (A24) are fulfilled and, furthermore, that ρ^e vanishes in the region of interest. Particularizing to a single temporal Fourier component of the field $\propto \exp(-i\omega t)$, we can then write $\mathbf{E} = -\partial\mathbf{A}/\partial t = i\omega\mathbf{A}$ and obtain the following expressions for the cycle averages of $\boldsymbol{\Sigma}^{\text{field}}$ and $\mathbf{L}^{\text{field}}$ in complex notation:

$$\langle \boldsymbol{\Sigma}^{\text{field}} \rangle_t = -i \frac{\epsilon_0}{2\omega} \int_V d^3x (\mathbf{E}^* \times \mathbf{E}) \tag{A52a}$$

$$\begin{aligned}
\langle \mathbf{L}^{\text{field}}(\mathbf{y}) \rangle_t &= -i \frac{\epsilon_0}{2\omega} \sum_{i=1}^3 \int_V d^3x E_i^* [(\mathbf{x} - \mathbf{y}) \times \nabla] E_i \\
&= \frac{\epsilon_0}{2\hbar\omega} \sum_{i=1}^3 \int_V d^3x E_i^* (-i\hbar \mathbf{x} \times \nabla) E_i \\
&\quad - \frac{\epsilon_0}{2\hbar\omega} \mathbf{y} \times \sum_{i=1}^3 \int_V d^3x E_i^* (-i\hbar \nabla) E_i \\
&= \langle \mathbf{L}^{\text{field}}(\mathbf{0}) \rangle_t - \mathbf{y} \times \langle \mathbf{p}^{\text{field}} \rangle_t
\end{aligned} \tag{A52b}$$

We note that if the cycle averaged electromagnetic field linear momentum $\langle \mathbf{p}^{\text{field}} \rangle_t \neq \mathbf{0}$, it is always possible to choose the moment point \mathbf{y} such that $\langle \mathbf{L}^{\text{field}}(\mathbf{y}) \rangle_t = \mathbf{0}$. But if $\langle \mathbf{p}^{\text{field}} \rangle_t = \mathbf{0}$, *i.e.*, if the cycle average of the linear momentum of the monochromatic field in question vanishes in a volume V , then

the cycle averaged OAM, $\langle \mathbf{L}^{\text{field}} \rangle_t$, is independent of \mathbf{y} in V . In a beam geometry the quantity Σ^{field} can often to a good approximation be identified with the spin angular momentum (SAM) carried by the field, and $\mathbf{L}^{\text{field}}$ with its orbital angular momentum (OAM).

The fact that we can express the temporal averages $\langle \mathbf{p}^{\text{field}} \rangle_t$ and $\langle \mathbf{L}^{\text{field}} \rangle_t$ in terms of expectation values with the quantal operators for linear and angular momentum, $\hat{\mathbf{p}}^{\text{field}} = -i\hbar\nabla$ and $\hat{\mathbf{L}}^{\text{field}} = -i\hbar\mathbf{x} \times \nabla$, respectively, hints to the first-quantization character of the Maxwell-Lorentz equations.

As is well known from quantum mechanics, but true also for classical fields, the Cartesian components of $\hat{\mathbf{L}}$ expressed in cylindrical coordinates (ρ, φ, z) are

$$\hat{L}_x^{\text{field}} = -i\hbar \left[\sin\varphi \left(z \frac{\partial}{\partial \rho} - \rho \frac{\partial}{\partial z} \right) + \frac{z}{\rho} \cos\varphi \frac{\partial}{\partial \varphi} \right] \quad (\text{A53a})$$

$$\hat{L}_y^{\text{field}} = -i\hbar \left[\cos\varphi \left(z \frac{\partial}{\partial \rho} - \rho \frac{\partial}{\partial z} \right) - \frac{z}{\rho} \sin\varphi \frac{\partial}{\partial \varphi} \right] \quad (\text{A53b})$$

$$\hat{L}_z^{\text{field}} = -i\hbar \frac{\partial}{\partial \varphi} \quad (\text{A53c})$$

duly recalling that \hbar should be divided out; cf. formula (A52b). The magnitude squared of the orbital angular momentum operator is

$$|\hat{\mathbf{L}}^{\text{field}}|^2 = (\hat{L}_x^{\text{field}})^2 + (\hat{L}_y^{\text{field}})^2 + (\hat{L}_z^{\text{field}})^2 \quad (\text{A54})$$

with eigenvalues $\hbar^2 l(l+1)$.

Orbital angular momentum is utilized in photonics and in optical trapping [90, 158–160] but has not yet been exploited fully in wireless communications. The conservation of angular momentum is a consequence of the rotational symmetry of electrodynamics.

4. Boost momentum

Due to the invariance of Maxwell's equations under Lorentz transformations, the first spatial momentum of the energy density (A1), and the linear momentum density (A10) multiplied by the elapsed time

$$\boldsymbol{\xi}(t, \mathbf{x}) = 2(\mathbf{x} - \mathbf{y})u^{\text{field}} - (t - t_0) \frac{1}{\epsilon_0} \mathbf{g}^{\text{field}} \quad (\text{A55})$$

fulfills a local (differential) conservation law. The integrated quantity

$$\mathbf{x}^{\text{ce}}(t) = \frac{\int_V d^3x \boldsymbol{\xi}(t, \mathbf{x})}{U^{\text{field}}} \quad (\text{A56})$$

is the center of energy [161]. Apparently this physical observable has not yet been exploited to any significant extent in radio or optics.

Appendix B: Hertzian dipoles

When the oscillations of an electric charge distribution $\rho^e(t', \mathbf{x}')$ are so small that their maximum amplitude (and the

largest extent of the smallest volume V' that fully encloses the charge distribution) is much smaller than the wavelength of the emitted fields, we can use the multipole expansion. The lowest order contribution to the fields comes from the electric monopole (charge) scalar

$$q^e(t') = \int_{V'} d^3x' \rho^e(t', \mathbf{x}') \quad (\text{B1})$$

The second lowest contribution comes from the electric (Hertzian) dipole moment vector with respect to an arbitrary moment point \mathbf{x}'_0 ,

$$\mathbf{d}(t', \mathbf{x}'_0) = \int_{V'} d^3x' (\mathbf{x}' - \mathbf{x}'_0) \rho^e(t', \mathbf{x}') \quad (\text{B2})$$

$$= \int_{V'} d^3x' \mathbf{x}' \rho^e(t', \mathbf{x}') - \mathbf{x}'_0 \int_{V'} d^3x' \rho^e(t', \mathbf{x}') \quad (\text{B3})$$

$$= \mathbf{d}(t', \mathbf{0}) - \mathbf{x}'_0 q^e(t') \quad (\text{B4})$$

Clearly there are two cases to consider here. If $q^e(t') \neq 0$, it is always possible to choose a moment point \mathbf{x}'_0 so that $\mathbf{d}(t', \mathbf{x}'_0) = \mathbf{0}$. But if $q^e(t') = 0$, then the dipole moment is independent of the choice of the moment point \mathbf{x}'_0 . Furthermore, since \mathbf{x}'_0 is a fix point,

$$\frac{\partial[\mathbf{d}(t', \mathbf{x}'_0)]}{\partial t'} = \frac{\partial[\mathbf{d}(t', \mathbf{x}'_0)]}{\partial t'} = \frac{\partial[\mathbf{d}(t', \mathbf{0})]}{\partial t'} - \mathbf{x}'_0 \frac{dq^e(t')}{dt'} \quad (\text{B5})$$

and, according to the equation of continuity for electric charge,

$$\frac{dq^e(t')}{dt'} = \int_{V'} d^3x' \frac{\partial \rho^e(t', \mathbf{x}')}{\partial t'} = - \oint_{S'} d^2x' \hat{\mathbf{n}}' \cdot \mathbf{j}^e(t', \mathbf{x}') \quad (\text{B6})$$

If there is no net flow of electric current across the surface S' that encloses V' , it therefore follows that

$$\frac{\partial[\mathbf{d}(t', \mathbf{x}'_0)]}{\partial t'} = \frac{\partial[\mathbf{d}(t', \mathbf{0})]}{\partial t'} \quad (\text{B7a})$$

$$\frac{\partial^2[\mathbf{d}(t', \mathbf{x}'_0)]}{\partial t'^2} = \frac{\partial^2[\mathbf{d}(t', \mathbf{0})]}{\partial t'^2} \quad (\text{B7b})$$

The electric and magnetic fields from an electric Hertzian dipole, oscillating at the angular frequency $\omega = ck$, where $k = \lambda/(2\pi)$ is the wave number, λ being the wavelength in free space, and located at the origin $\mathbf{x}' = \mathbf{0}$, which is also the moment point chosen,

$$\mathbf{d}(t', \mathbf{0}) = \mathbf{d}_\omega(\mathbf{0}) e^{-i(\omega t' + \delta)} \quad (\text{B8})$$

where $\delta = \omega \Delta t'$ is an arbitrary constant phase, can be obtained from Eqns. (28).

We apply the decomposition (26) on $\mathbf{d}_\omega(\mathbf{0})$, resulting in a parallel (\parallel), and a perpendicular (\perp) component

$$\mathbf{d}_\parallel(\mathbf{0}) = [\mathbf{d}_\omega(\mathbf{0}) \cdot \hat{\mathbf{n}}'] \hat{\mathbf{n}}' \quad (\text{B9})$$

$$\mathbf{d}_\perp(\mathbf{0}) = \mathbf{d}_\omega(\mathbf{0}) - \mathbf{d}_\parallel = \mathbf{d}_\omega - [\mathbf{d}_\omega(\mathbf{0}) \cdot \hat{\mathbf{n}}'] \hat{\mathbf{n}}' \quad (\text{B10})$$

Using a spherical coordinate system (r, ϑ, φ) where $\hat{\mathbf{r}} \equiv \hat{\mathbf{n}}'$ and, from Eqn. (22), $t' = t - r/c$, the fields generated by \mathbf{d} can be

written [cf. Cohen-Tannoudji *et al.* [40, Eqn. (16), p. 73]]

$$\mathbf{E}(t, \mathbf{x}) = \frac{\mathbf{d}_{\parallel}(\mathbf{0})}{2\pi\epsilon_0} [f_2(\delta) + f_3(\delta)] + \frac{\mathbf{d}_{\perp}(\mathbf{0})}{4\pi\epsilon_0} [f_1(\delta) - f_2(\delta) - f_3(\delta)] \quad (\text{B11a})$$

$$\mathbf{B}(t, \mathbf{x}) = \frac{\hat{\mathbf{r}} \times \mathbf{d}_{\perp}(\mathbf{0})}{4\pi\epsilon_0 c} [f_1(\delta) - f_2(\delta)] \quad (\text{B11b})$$

where, for convenience and compactness, we introduced the help quantities

$$f_1(\delta) \equiv f_1(\omega t', \delta) = \frac{k^2}{r} \cos(kr - \omega t + \delta) \quad (\text{B12a})$$

$$f_2(\delta) \equiv f_2(\omega t', \delta) = \frac{k}{r^2} \sin(kr - \omega t + \delta) \quad (\text{B12b})$$

$$f_3(\delta) \equiv f_3(\omega t', \delta) = \frac{1}{r^3} \cos(kr - \omega t + \delta) \quad (\text{B12c})$$

with the subscript n denoting how the component f_n in question behaves as a power of radial distance r from the dipole, *i.e.*, $\mathcal{O}(f_n) = r^{-n}$.

1. Hertzian dipoles directed along the three Cartesian axes

Let us now consider three Hertzian dipoles directed along the three Cartesian axes. We denote their (Fourier) amplitudes

$$\mathbf{d}_j(\mathbf{0}) \equiv \mathbf{d}_{j\omega}(\mathbf{0}) = d_{j\omega}(\mathbf{0}) \hat{\mathbf{x}}_j, j = 1, 2, 3. \quad (\text{B13})$$

where $\hat{\mathbf{x}}_1 = \hat{\mathbf{x}}$, $\hat{\mathbf{x}}_2 = \hat{\mathbf{y}}$, and $\hat{\mathbf{x}}_3 = \hat{\mathbf{z}}$.

a. Electric and magnetic fields The individual electric Hertzian dipoles $\mathbf{d}_j(\mathbf{0})$, $j = 1, 2, 3$, generate electric and magnetic field vectors \mathbf{E}_j and \mathbf{B}_j . In spherical polar coordinates they are:

$$\begin{aligned} \mathbf{E}_1(t, \mathbf{x}) &= \frac{d_1(\mathbf{0})}{2\pi\epsilon_0} [f_2(\delta_1) + f_3(\delta_1)] \sin \vartheta \cos \varphi \hat{\boldsymbol{\rho}} \\ &+ \frac{d_1(\mathbf{0})}{4\pi\epsilon_0} [f_1(\delta_1) - f_2(\delta_1) - f_3(\delta_1)] \cos \vartheta \cos \varphi \hat{\boldsymbol{\theta}} \\ &- \frac{d_1(\mathbf{0})}{4\pi\epsilon_0} [f_1(\delta_1) - f_2(\delta_1) - f_3(\delta_1)] \sin \varphi \hat{\boldsymbol{\phi}} \quad (\text{B14a}) \end{aligned}$$

$$\begin{aligned} \mathbf{B}_1(t, \mathbf{x}) &= \frac{d_1(\mathbf{0})}{4\pi\epsilon_0 c} [f_1(\delta_1) - f_2(\delta_1)] \sin \varphi \hat{\boldsymbol{\theta}} \\ &+ \frac{d_1(\mathbf{0})}{4\pi\epsilon_0 c} [f_1(\delta_1) - f_2(\delta_1)] \cos \vartheta \cos \varphi \hat{\boldsymbol{\phi}} \quad (\text{B14b}) \end{aligned}$$

$$\begin{aligned} \mathbf{E}_2(t, \mathbf{x}) &= \frac{d_2(\mathbf{0})}{2\pi\epsilon_0} [f_2(\delta_2) + f_3(\delta_2)] \sin \vartheta \sin \varphi \hat{\boldsymbol{\rho}} \\ &+ \frac{d_2(\mathbf{0})}{4\pi\epsilon_0} [f_1(\delta_2) - f_2(\delta_2) - f_3(\delta_2)] \cos \vartheta \sin \varphi \hat{\boldsymbol{\theta}} \\ &+ \frac{d_2(\mathbf{0})}{4\pi\epsilon_0} [f_1(\delta_2) - f_2(\delta_2) - f_3(\delta_2)] \cos \varphi \hat{\boldsymbol{\phi}} \quad (\text{B14c}) \end{aligned}$$

$$\begin{aligned} \mathbf{B}_2(t, \mathbf{x}) &= -\frac{d_2(\mathbf{0})}{4\pi\epsilon_0 c} [f_1(\delta_2) - f_2(\delta_2)] \cos \varphi \hat{\boldsymbol{\theta}} \\ &+ \frac{d_2(\mathbf{0})}{4\pi\epsilon_0 c} [f_1(\delta_2) - f_2(\delta_2)] \cos \vartheta \sin \varphi \hat{\boldsymbol{\phi}} \quad (\text{B14d}) \end{aligned}$$

$$\begin{aligned} \mathbf{E}_3(t, \mathbf{x}) &= \frac{d_3(\mathbf{0})}{2\pi\epsilon_0} [f_2(\delta_3) + f_3(\delta_3)] \cos \vartheta \hat{\boldsymbol{\rho}} \\ &- \frac{d_3(\mathbf{0})}{4\pi\epsilon_0} [f_1(\delta_3) - f_2(\delta_3) - f_3(\delta_3)] \sin \vartheta \hat{\boldsymbol{\theta}} \quad (\text{B14e}) \end{aligned}$$

$$\mathbf{B}_3(t, \mathbf{x}) = -\frac{d_3(\mathbf{0})}{4\pi\epsilon_0 c} [f_1(\delta_3) - f_2(\delta_3)] \sin \vartheta \hat{\boldsymbol{\phi}} \quad (\text{B14f})$$

b. Vector products of the fields When we want to calculate the linear and angular momenta carried by the fields radiated by Hertzian dipoles directed along the Cartesian axes, we need to evaluate expressions that involve the vector products $\mathbf{E}_j \times \mathbf{B}_k$ for various combinations of $j, k = 1, 2, 3$. Here we list a few such vector products.

$$\begin{aligned} \mathbf{E}_1 \times \mathbf{B}_1 &= \frac{d_1^2(\mathbf{0})}{16\pi^2\epsilon_0^2 c} [f_1^2(\delta_1) - 2f_1(\delta_1)f_2(\delta_1) \\ &- f_1(\delta_1)f_3(\delta_1) + f_2^2(\delta_1) \\ &+ f_2(\delta_1)f_3(\delta_1)] (1 - \sin^2 \vartheta \cos^2 \varphi) \hat{\boldsymbol{\rho}} \\ &- \frac{d_1^2(\mathbf{0})}{8\pi^2\epsilon_0^2 c} [f_1(\delta_1)f_2(\delta_1) + f_1(\delta_1)f_3(\delta_1) \\ &- f_2^2(\delta_1) - f_2(\delta_1)f_3(\delta_1)] \sin \vartheta \cos \vartheta \cos^2 \varphi \hat{\boldsymbol{\theta}} \\ &+ \frac{d_1^2(\mathbf{0})}{8\pi^2\epsilon_0^2 c} [f_1(\delta_1)f_2(\delta_1) + f_1(\delta_1)f_3(\delta_1) \\ &- f_2^2(\delta_1) - f_2(\delta_1)f_3(\delta_1)] \sin \vartheta \sin \varphi \cos \varphi \hat{\boldsymbol{\phi}} \quad (\text{B15}) \end{aligned}$$

$$\begin{aligned} \mathbf{E}_2 \times \mathbf{B}_2 &= \frac{d_2^2(\mathbf{0})}{16\pi^2\epsilon_0^2 c} [f_1^2(\delta_2) - 2f_1(\delta_2)f_2(\delta_2) \\ &- f_1(\delta_2)f_3(\delta_2) + f_2^2(\delta_2) \\ &+ f_2(\delta_2)f_3(\delta_2)] (1 - \sin^2 \vartheta \sin^2 \varphi) \hat{\boldsymbol{\rho}} \\ &- \frac{d_2^2(\mathbf{0})}{8\pi^2\epsilon_0^2 c} [f_1(\delta_2)f_2(\delta_2) + f_1(\delta_2)f_3(\delta_2) \\ &- f_2^2(\delta_2) - f_2(\delta_2)f_3(\delta_2)] \sin \vartheta \cos \vartheta \sin^2 \varphi \hat{\boldsymbol{\theta}} \\ &- \frac{d_2^2(\mathbf{0})}{8\pi^2\epsilon_0^2 c} [f_1(\delta_2)f_2(\delta_2) + f_1(\delta_2)f_3(\delta_2) \\ &- f_2^2(\delta_2) - f_2(\delta_2)f_3(\delta_2)] \sin \vartheta \sin \varphi \cos \varphi \hat{\boldsymbol{\phi}} \quad (\text{B16}) \end{aligned}$$

$$\begin{aligned} \mathbf{E}_3 \times \mathbf{B}_3 &= \frac{d_3^2(\mathbf{0})}{16\pi^2 \varepsilon_0^2 c} [f_1^2(\delta_3) - 2f_1(\delta_3)f_2(\delta_3) + f_2^2(\delta_3) \\ &\quad - f_1(\delta_3)f_3(\delta_3) + f_2(\delta_3)f_3(\delta_3)] \sin^2 \vartheta \hat{\mathbf{r}} \\ &\quad + \frac{d_3^2(\mathbf{0})}{8\pi^2 \varepsilon_0^2 c} [f_1(\delta_3)f_2(\delta_3) + f_1(\delta_3)f_3(\delta_3) \\ &\quad - f_2^2(\delta_3) - f_2(\delta_3)f_3(\delta_3)] \sin \vartheta \cos \vartheta \hat{\boldsymbol{\theta}} \quad (\text{B17}) \end{aligned}$$

$$\begin{aligned} \mathbf{E}_1 \times \mathbf{B}_2 &= -\frac{d_1(\mathbf{0})d_2(\mathbf{0})}{16\pi^2 \varepsilon_0^2 c} [f_1(\delta_1)f_1(\delta_2) - f_1(\delta_1)f_2(\delta_2) \\ &\quad - f_1(\delta_2)f_2(\delta_1) - f_1(\delta_2)f_3(\delta_1) \\ &\quad + f_2(\delta_1)f_2(\delta_2) + f_2(\delta_2)f_3(\delta_1)] (1 - \cos^2 \vartheta) \sin \varphi \cos \varphi \hat{\mathbf{r}} \\ &\quad - \frac{d_1(\mathbf{0})d_2(\mathbf{0})}{8\pi^2 \varepsilon_0^2 c} [f_1(\delta_2)f_2(\delta_1) + f_1(\delta_2)f_3(\delta_1) \\ &\quad - f_2(\delta_1)f_2(\delta_2) - f_2(\delta_2)f_3(\delta_1)] \sin \vartheta \cos \vartheta \sin \varphi \cos \varphi \hat{\boldsymbol{\theta}} \\ &\quad - \frac{d_1(\mathbf{0})d_2(\mathbf{0})}{8\pi^2 \varepsilon_0^2 c} [f_1(\delta_2)f_2(\delta_1) + f_1(\delta_2)f_3(\delta_1) \\ &\quad - f_2(\delta_1)f_2(\delta_2) - f_2(\delta_2)f_3(\delta_1)] \sin \vartheta \cos^2 \vartheta \hat{\boldsymbol{\phi}} \quad (\text{B18}) \end{aligned}$$

$$\begin{aligned} \mathbf{E}_2 \times \mathbf{B}_1 &= -\frac{d_1(\mathbf{0})d_2(\mathbf{0})}{16\pi^2 \varepsilon_0^2 c} [f_1(\delta_1)f_1(\delta_2) - f_1(\delta_1)f_2(\delta_2) \\ &\quad - f_1(\delta_2)f_2(\delta_1) - f_1(\delta_1)f_3(\delta_2) \\ &\quad + f_2(\delta_1)f_2(\delta_2) + f_2(\delta_1)f_3(\delta_2)] (1 - \cos^2 \vartheta) \sin \varphi \cos \varphi \hat{\mathbf{r}} \\ &\quad - \frac{d_1(\mathbf{0})d_2(\mathbf{0})}{8\pi^2 \varepsilon_0^2 c} [f_1(\delta_1)f_2(\delta_2) + f_1(\delta_1)f_3(\delta_2) \\ &\quad - f_2(\delta_1)f_2(\delta_2) - f_2(\delta_1)f_3(\delta_2)] \sin \vartheta \cos \vartheta \sin \varphi \cos \varphi \hat{\boldsymbol{\theta}} \\ &\quad + \frac{d_1(\mathbf{0})d_2(\mathbf{0})}{8\pi^2 \varepsilon_0^2 c} [f_1(\delta_1)f_2(\delta_2) + f_1(\delta_1)f_3(\delta_2) \\ &\quad - f_2(\delta_1)f_2(\delta_2) - f_2(\delta_1)f_3(\delta_2)] \sin \vartheta \sin^2 \vartheta \hat{\boldsymbol{\phi}} \quad (\text{B19}) \end{aligned}$$

-
- [1] P. A. M. Dirac, "Quantised singularities in the electromagnetic field," *Proc. Roy. Soc. London Ser. A Math. Phys. Sci.* **133**, 60–72 (1931).
- [2] Julian Schwinger, "A magnetic model of matter," *Science* **165**, 757–761 (1969).
- [3] Julian Schwinger, Lester L. DeRaad, Jr., Kimball A. Milton, and Wu-yang Tsai, *Classical Electrodynamics* (Perseus Books, Reading, MA, USA, 1998).
- [4] John David Jackson, *Classical Electrodynamics*, 3rd ed. (Wiley & Sons, New York, NY, USA, 1998).
- [5] B. ThidAl, Nicholas M. Elias, II, F. Tamburini, S. M. Mohammadi, and J. T. Mendonca, "Applications of electromagnetic OAM in astrophysics and space physics studies," in *Twisted Photons: Applications of Light With Orbital Angular Momentum*, edited by Juan P. Torres and Llus Torner (Wiley-Vch Verlag, Weinheim, DE, 2011) Chap. 9, pp. 155–178.
- [6] Bo Thide, *Electromagnetic Field Theory*, 2nd ed. (Dover Publications, Inc., Mineola, NY, USA, 2011) (In press).
- [7] Heinrich Weber, *Die partiellen Differential-Gleichungen der mathematischen Physik nach Riemann's Vorlesungen* (Friedrich Vieweg und Sohn, Braunschweig, 1901).
- [8] Ludwik Silberstein, "Elektromagnetische Grundgleichungen in bivectorieller Behandlung," *Ann. Phys. (Leipzig)* **327**, 579–586 (1907).
- [9] Ludwik Silberstein, "Nachtrag zur Abhandlung ber elektromagnetische Grundgleichungen in bivectorieller Behandlung," *Ann. Phys. (Leipzig)* **329**, 783–784 (1907).
- [10] Ludwik Silberstein, *The Theory of Relativity* (MacMillan, London, 1914).
- [11] Harry Bateman, *The Mathematical Analysis of Electrical and Optical Wave-Motion on the Basis of Maxwell's Equations* (Cambridge University Press, Cambridge, UK, 1915).
- [12] Iwo Bialynicki-Birula and Zofia Bialynicka-Birula, "Beams of electromagnetic radiation carrying angular momentum: The Riemann-Silberstein vector and the classical-quantum correspondence," *Opt. Commun.* **264**, 342–351 (2006).
- [13] Iwo Bialynicki-Birula and Zofia Bialynicka-Birula, "Why photons cannot be sharply localized," *Phys. Rev. A* **79**, 032112 (2009).
- [14] Donald H. Kobe, "A relativistic Schrodinger-like equation for a photon and its second quantization," *Found. Phys.* **29**, 1203–1231 (1999).
- [15] Ettore Majorana, "Research notes on theoretical physics," (2009), unpublished, deposited at the 'Domus Galileana,' Pisa, quaderno 2, p. 101/1; 3, p. 11, 160; 15, p. 16; 17, p. 83, 159.
- [16] J. R. Oppenheimer, "Note on light quanta and the electromagnetic field," *Phys. Rev.* **38**, 725–746 (1931).
- [17] Otto Laporte and George E. Uhlenbeck, "Application of spinor analysis to the Maxwell and Dirac equations," *Phys. Rev.* **37**, 1380–1397 (1931).
- [18] W. J. Archibald, "Field equations from particle equations," *Canadian Journal of Physics* **33**, 565–572 (1955).
- [19] R. H. Good, "Particle aspect of the electromagnetic field equations," *Phys. Rev.* **105**, 1914–1918 (1957).
- [20] H. E. Moses, "Solution of Maxwell's equations in terms of a spinor notation: the direct and inverse problem," *Phys. Rev.* **113**, 1670–1679 (1959).
- [21] Behram Kursunoglu, "Complex orthogonal and antiorthogonal representation of Lorentz group," *J. Math. Phys.* **2**, 22–32 (1961).
- [22] R. Mignani, E. Recami, and M. Baldo, "About a Dirac-like equation for the photon according to Ettore Majorana," *Lett.*

- Nuov. Cim. **11**, 568–572 (1974).
- [23] Asim O. Barut, *Electrodynamics and Classical Theory of Fields and Particles* (Dover Publications, New York, NY, USA, 1980).
- [24] E. Giannetto, “A Majorana–Oppenheimer formulation of quantum electrodynamics,” *Lett. Nuov. Cim.* **2**, **44**, 140–144 (1985).
- [25] J. E. Sipe, “Photon wave functions,” *Phys. Rev. A* **52**, 1875–1883 (1995).
- [26] Iwo Białynicki-Birula, “On the wave function of the photon,” *Acta Phys. Polon.* **A 86**, 97–116 (1994).
- [27] I. Białynicki-Birula, “Photon wave function,” in *Prog. Opt.*, Vol. XXXVI, edited by E. Wolf (Elsevier, Amsterdam, Holland, 1996) pp. 245–294.
- [28] S. Esposito, “Covariant Majorana formulation of electrodynamics,” *Found. Phys.* **28**, 231–244 (1998).
- [29] A. Gersten, “Maxwell equations—the one-photon quantum equation,” *Found. Phys. Lett.* **12**, 291–298 (1999).
- [30] Ole Keller, “On the theory of spatial localization of photons,” *Phys. Rep.* **411**, 1–232 (2005).
- [31] Sameen Ahmed Khan, “An exact matrix representation of Maxwell’s equations,” *Phys. Scr.* **71**, 440–442 (2005).
- [32] Daniela Dragoman, “Photon states from propagating complex electromagnetic fields,” *J. Opt. Soc. Am. B* **24**, 922–927 (2007).
- [33] F. Tamburini and D. Vicino, “Photon wave function: A covariant formulation and equivalence with QED,” *Phys. Rev. A* **78**, 052116(5) (2008).
- [34] A. A. Bogush, G. G. Krylov, E. M. Ovsyuk, and V. M. Red’kov, “Maxwell equations in complex form of Majorana–Oppenheimer, solutions with cylindric symmetry in Riemann S_3 and Lobachevsky H_3 spaces,” *Ricerche Mat.* **59**, 59–96 (2009).
- [35] Zhi-Yong Wang, Cai-Dong Xiong, and Qi Qiu, “Photon wave function and Zitterbewegung,” *Phys. Rev. A* **80**, 032118 (2009).
- [36] Peter J. Mohr, “Solutions of the Maxwell equations and photon wave functions,” *Ann. Phys. (N. Y.)* **325**, 607–663 (2010).
- [37] Andreas Aste, “Complex representation theory of the electromagnetic field,” *J. Geom. Sym. Phys.* **28**, 47–58 (2012).
- [38] Takuo Yamamoto, Shinji Yamashita, and Satoshi Yajima, “Wave function of a photon and the appropriate Lagrangian,” *J. Phys. Soc. Japan* **81**, 024402 (2012).
- [39] Iwo Białynicki-Birula and Zofia Białynicka-Birula, “The role of the Riemann–Silberstein vector in classical and quantum theories of electromagnetism,” *J. Phys. A: Math. Gen.* **46**, 053001 (2013).
- [40] Claude Cohen-Tannoudji, Jaques Dupont-Roc, and Gilbert Grynberg, *Photons and Atoms. Introduction to Quantum Electrodynamics* (Wiley & Sons, New York, NY, USA, 1997) Wiley Professional Paperback Edition.
- [41] Freeman J. Dyson, “Why is Maxwell’s Theory so hard to understand?” in *James Clerk Maxwell Commemorative Booklet* (James Clerk Maxwell Foundation, Edinburgh, Scotland, UK, 1999) <http://www.clerkmaxwellfoundation.org/DysonFreemanArticle.pdf>.
- [42] Daniel M. Siegel, *Innovation in Maxwell’s Electromagnetic Theory: Molecular Vortices, Displacement Current, and Light* (Cambridge University Press, Cambridge, UK, 2003).
- [43] A. I. Sadovskii, “Ponderomotorniya djstviya elektromagnitnykh’ i svtovykh’ voln’,” *Uchen. Zapis. Imp. Yurev. Univ.* **52**, 1–126 (1899).
- [44] J. H. Poynting, “The wave motion of a revolving shaft, and a suggestion as to the angular momentum in a beam of circularly polarised light,” *Proc. Roy. Soc. London* **A 82**, 560–567 (1909).
- [45] Max Abraham, “Der Drehimpuls des Lichtes,” *Physik. Zeitschr.* **XV**, 914–918 (1914).
- [46] H. Bateman, “The radiation of energy and angular momentum,” *Phys. Rev.* **27**, 606–617 (1926).
- [47] Walter Heitler, *The Quantum Theory of Radiation*, 3rd ed., The International Series of Monographs on Physics (Clarendon Press, Oxford, UK, 1954).
- [48] N. N. Bogolyubov and D. V. Shirkov, *Introduction to the Theory of Quantized Fields* (Interscience, New York, 1959).
- [49] Albert Messiah, *Quantum Mechanics* (North-Holland, Amsterdam, NL, 1970).
- [50] Leonard Eyges, *The Classical Electromagnetic Field* (Dover Publications, New York, NY, USA, 1972).
- [51] L. D. Landau and E. M. Lifshitz, *The Classical Theory of Fields*, Course of Theoretical Physics, Vol. 2 (Pergamon, Oxford, UK, 1975).
- [52] V. B. Berestetskii, E. M. Lifshitz, and L. P. Pitaevskii, *Quantum Electrodynamics*, 2nd ed., Course of Theoretical Physics, Vol. 4 (Pergamon Press, Oxford, UK, 1989).
- [53] Leonard Mandel and Emil Wolf, *Optical Coherence and Quantum Optics* (Cambridge University Press, New York, NY, USA, 1995).
- [54] David J. Griffiths, *Introduction to Electrodynamics*, 3rd ed. (Prentice-Hall International, London, UK, 1999).
- [55] Fritz Rohrlich, *Classical Charged Particles*, 3rd ed. (World Scientific, Singapore, 2007).
- [56] Graham Gibson, Johannes Courtial, Miles J. Padgett, Mikhail Vasnetsov, Valeriy Pas’ko, Stephen M. Barnett, and Sonja Franke-Arnold, “Free-space information transfer using light beams carrying orbital angular momentum,” *Opt. Express* **12**, 5448–5456 (2004).
- [57] B. Thidé, H. Then, J. Sjöholm, K. Palmer, J. Bergman, T. D. Carozzi, Ya. N. Istomin, N. H. Ibragimov, and R. Khamitova, “Utilization of photon orbital angular momentum in the low-frequency radio domain,” *Phys. Rev. Lett.* **99**, 087701(4) (2007).
- [58] S. Franke-Arnold, L. Allen, and M. Padgett, “Advances in optical angular momentum,” *Laser & Photon. Rev.* **2**, 299–313 (2008).
- [59] Fabrizio Tamburini, Bo Thidé, Gabriel Molina-Terriza, and Gabriele Anzolin, “Twisting of light around rotating black holes,” *Nature Phys.* **7**, 195–197 (2011).
- [60] Fabrizio Tamburini, Elettra Mari, Bo Thidé, Cesare Barbieri, and Filippo Romanato, “Experimental verification of photon angular momentum and vorticity with radio techniques,” *Appl. Phys. Lett.* **99**, 204102 (2011).
- [61] Fabrizio Tamburini, Elettra Mari, Anna Sponselli, Bo Thidé, Antonio Bianchini, and Filippo Romanato, “Encoding many channels on the same frequency through radio vorticity: first experimental test,” *New J. Phys.* **14**, 03301 (2012).
- [62] F. Tamburini, B. Thidé, E. Mari, A. Sponselli, A. Bianchini, and F. Romanato, “Reply to comment on ‘Encoding many channels on the same frequency through radio vorticity: first experimental test’,” *New J. Phys.* **14**, 118002 (2012).
- [63] Graham Gibson, Johannes Courtial, Mikhail Vasnetsov, Stephen Barnett, and Sonja Franke-Arnold, “Increasing the data density of free-space optical communications using orbital angular momentum,” in *Free-Space Laser Communications IV*, Proceedings of SPIE, Vol. 5550, edited by Jennifer C. Rickling and David G. Voetz (Denver, CO, USA, 2004) pp. 367–373.
- [64] Jian Wang, Jeng-Yuan Yang, Irfan M. Fazal, Nisar Ahmed, Yan Yan, Hao Huang, Yongxiong Ren, Yang Yue, Samuel Dolinar, Moshe Tur, and Alan E. Willner, “Terabit free-space data transmission employing orbital angular momentum multiplexing,” *Nature Photon.* **6**, 488–496 (2012).

- [65] Natalia M. Litchinitser, “Structured light meets structured matter,” *Science* **337**, 1054–1055 (2012).
- [66] Nenad Bozinovic, Yang Yue, Yongxiong Ren, Moshe Tur, Poul Kristensen, Hao Huang, Alan E. Willner, and Siddharth Ramachandran, “Terabit-scale orbital angular momentum mode division multiplexing in fibers,” *Science* **340**, 1545–1548 (2013).
- [67] Yan Yan, Guodong Xie, Martin P. J. Lavery, Hao Huang, Nisar Ahmed, Changjing Bao, Yongxiong Ren, Yinwen Cao, Long Li, Zhe Zhao, Andreas F. Molisch, Moshe Tur, Miles J. Padgett, and Alan E. Willner, “High-capacity millimetre-wave communications with orbital angular momentum multiplexing,” *Nature Commun.* **5**, 1–9 (2014).
- [68] M. V. Berry, “Optical vortices evolving from helicoidal integer and fractional phase steps,” *J. Opt. A: Pure Appl. Opt.* **6**, 259–268 (2004).
- [69] R. Čelechovský and Z. Bouchal, “Optical implementation of the vortex information channel,” *New J. Phys.* **9**, 328 (2007).
- [70] Julio T. Barreiro, Tzu-Chieh Wei, and Paul G. Kwiat, “Beating the channel capacity limit for linear photonic superdense coding,” *Nature Phys.* **4**, 282–286 (2008).
- [71] J. B. Pors, S. S. R. Oemrawsingh, A. Aiello, M. P. van Exter, E. R. Eliel, G. W. ’t Hooft, and J. P. Woerdman, “Shannon dimensionality of quantum channels and its application to photon entanglement,” *Phys. Rev. Lett.* **101**, 120502 (2008).
- [72] P. Martelli, A. Gatto, P. Boffi, and M. Martinelli, “Free-space optical transmission with orbital angular momentum division multiplexing,” *Electron. Lett.* **47**, 972–973 (2011).
- [73] Ashok Kumar, Shashi Prabhakar, Pravin Vaity, and R. P. Singh, “Information content of optical vortex fields,” *Opt. Lett.* **36**, 1161–1163 (2011).
- [74] N. Bohr, “On the constitution of atoms and molecules,” *Philos. Mag.* **6**, **26**, 1–25 (1913).
- [75] Arnold Sommerfeld, *Atombau und Spektrallinien* (F. Vieweg & Sohn, 1921).
- [76] David Bohm, *Quantum Theory* (Dover Publications Inc., New York, 1989).
- [77] Gerard Nienhuis, “Angular momentum and vortices in optics,” in *Structured Light and its Applications: An Introduction to Phase-Structured Beams and Nanoscale Optical Forces* (Elsevier Inc., Amsterdam, NL, 2008) pp. 19–61.
- [78] A. Mair, A. Vaziri, G. Weihs, and A. Zeilinger, “Entanglement of the orbital angular momentum states of photons,” *Nature* **412**, 313–316 (2001).
- [79] Andrew Watson, “New twist could pack photons with data,” *Science* **296**, 2316–2317 (2002).
- [80] Lluís Torner, Juan P. Torres, and Silvia Carrasco, “Digital spiral imaging,” *Opt. Express* **13**, 873–881 (2005).
- [81] Gabriel Molina-Terriza, Juan P. Torres, and Lluís Torner, “Management of the angular momentum of light: Preparation of photons in multidimensional vector states of angular momentum,” *Phys. Rev. Lett.* **88**, 013601(4) (2002).
- [82] Branka Vucetic and Jinhong Yuan, *Space-Time Coding* (John Wiley & Sons, UK, 2003).
- [83] Pierpaolo Boffi, P. Martelli, A. Gatto, and M. Martinelli, “Optical vortices: an innovative approach to increase spectral efficiency by fiber mode-division multiplexing,” in *Next-Generation Optical Communication: Components, Sub-Systems, and Systems I*, Proc. of SPIE, Vol. 8647 (San Francisco, CA, USA, 2013) pp. 864705–864705–8.
- [84] F. J. Belinfante, “On the current and the density of the electric charge, the energy, the linear momentum and the angular momentum of arbitrary fields,” *Physica* **7**, 449–474 (1940).
- [85] Davison E. Soper, *Classical Field Theory* (John Wiley & Sons, Inc., New York, NY, USA, 1976).
- [86] Clifford Truesdell, *Essays in the History of Mechanics* (Springer-Verlag, Berlin, Heidelberg, New York, 1968).
- [87] Marijan Ribarič and Luka Šušteršič, *Conservation Laws and Open Questions of Classical Electrodynamics* (World Scientific, Singapore, New Jersey, London, Hong Kong, 1990).
- [88] L. Allen, S. M. Barnett, and M. J. Padgett, *Optical Angular Momentum* (IOP, Bristol, UK, 2003).
- [89] David L. Andrews, *Structured Light and Its Applications: An Introduction to Phase-Structured Beams and Nanoscale Optical Forces* (Academic Press, Amsterdam, NL, 2008).
- [90] Juan P. Torres and Lluís Torner, *Twisted Photons: Applications of Light With Orbital Angular Momentum* (Wiley-Vch Verlag, John Wiley and Sons, Weinheim, DE, 2011).
- [91] Alison M. Yao and Miles J. Padgett, “Orbital angular momentum: origins, behavior and applications,” *Adv. Opt. Photon.* **3**, 161–204 (2011).
- [92] Richard A. Beth, “Direct detection of the angular momentum of light,” *Phys. Rev.* **48**, 471 (1935).
- [93] Richard A. Beth, “Mechanical detection and measurement of the angular momentum of light,” *Phys. Rev.* **50**, 115–125 (1936).
- [94] A. H. S. Holbourn, “Angular momentum of circularly polarised light,” *Nature* **137**, 31–31 (1936).
- [95] Nello Carrara, “Torque and angular momentum of centimetre electromagnetic waves,” *Nature* **164**, 882–884 (1949).
- [96] P. J. Allen, “A radiation torque experiment,” *Am. J. Phys.* **34**, 1185–1192 (1966).
- [97] S. Carusotto, G. Fornaca, and E. Polacco, “Radiation beats and rotating systems,” *Nuov. Cim.* **53**, 87–97 (1968).
- [98] Soo Chang and Sang Soo Lee, “Optical torque exerted on a homogeneous sphere levitated in the circularly polarized fundamental-mode laser beam,” *J. Opt. Soc. Am. B* **2**, 1853–1860 (1985).
- [99] K. S. Vul’fson, “Angular momentum of electromagnetic waves,” *Sov. Phys. Usp.* **30**, 667–674 (1987).
- [100] M. Kristensen, M. W. Beijersbergen, and J. P. Woerdman, “Angular momentum and spin-orbit coupling for microwave photons,” *Opt. Commun.* **104**, 229–233 (1994).
- [101] H. He, M. E. J. Friese, N. R. Heckenberg, and H. Rubinsztein-Dunlop, “Direct observation of transfer of angular momentum to absorptive particles from a laser beam with a phase singularity,” *Phys. Rev. Lett.* **75**, 826–829 (1995).
- [102] M. E. J. Friese, J. Enger, H. Rubinsztein-Dunlop, and N. R. Heckenberg, “Optical angular-momentum transfer to trapped absorbing particles,” *Phys. Rev. A* **54**, 1593–1596 (1996).
- [103] H. Then and B. Thidé, “Mechanical properties of the radio frequency field emitted by an antenna array,” (2008), arXiv.org:0803.0200 [physics.class-ph].
- [104] K. Helmersson, M. F. Andersen, P. Cladé, V. Natarajan, W. D. Phillips, A. Ramanathan, C. Ryu, and A. Vaziri, “Vortices and persistent currents: Rotating a Bose-Einstein condensate using photons with orbital angular momentum,” *Topologica* **2**, 002–1–002–12 (2009).
- [105] Miles Padgett and Richard Bowman, “Tweezers with a twist,” *Nature Phys.* **5**, 343–348 (2011).
- [106] A. Ramanathan, K. C. Wright, S. R. Muniz, M. Zelan, W. T. Hill, C. J. Lobb, K. Helmersson, W. D. Phillips, and G. K. Campbell, “Superflow in a toroidal Bose-Einstein condensate: An atom circuit with a tunable weak link,” *Phys. Rev. Lett.* **106**, 130401 (2011).
- [107] Nicholas M. Elias, II, “Photon orbital angular momentum and torque metrics for single telescopes and interferometers,” *Astron. Astrophys.* **541**, A101 (2012).

- [108] Olivier Emile, Christian Brousseau, Janine Emile, Ronan Niemiec, Kouros Madhjoubi, and Bo Thidé, “Electromagnetically induced torque on a large ring in the microwave range,” *Phys. Rev. Lett.* **112**, 053902(4) (2014).
- [109] Gabriel Molina-Terriza, Liis Rebane, Juan P. Torres, Lluís Torner, and Silvia Carrasco, “Probing canonical geometrical objects by digital spiral imaging,” *J. Eur. Opt. Soc.* **2**, 07014(6) (2007).
- [110] B. Thidé, “Nonlinear physics of the ionosphere and LOIS/LOFAR,” *Plasma Phys. Contr. Fusion* **49**, B103–B107 (2007).
- [111] J. T. Mendonça, B. Thidé, J. E. S. Bergman, S. M. Mohammadi, B. Eliasson, W. Baan, and H. Then, “Photon orbital angular momentum in a plasma vortex,” (2008), arXiv.org:0804.3221 [physics.plasm-ph].
- [112] J. T. Mendonça, B. Thidé, and H. Then, “Stimulated Raman and Brillouin backscattering of collimated beams carrying orbital angular momentum,” *Phys. Rev. Lett.* **102**, 185005(4) (2009).
- [113] F. Tamburini, A. Sponselli, B. Thidé, and J. T. Mendonça, “Photon orbital angular momentum and mass in a plasma vortex,” *Europhys. Lett.* **90**, 45001 (2010).
- [114] F. Tamburini and B. Thidé, “Storming Majorana’s Tower with OAM states of light in a plasma,” *Europhys. Lett.* **96**, 64005 (2011).
- [115] J. T. Mendonça, “Twisted waves in a plasma,” *Plasma Phys. Contr. Fusion* **54**, 124031 (2012).
- [116] M. Ibanescu, Y. Fink, S. Fan, E. L. Thomas, and J. D. Joannopoulos, “An all-dielectric coaxial waveguide,” *Science* **289**, 415–419 (2000).
- [117] Julius Adams Stratton, *Electromagnetic Theory* (McGraw-Hill Book Co., New York, NY, USA, 1941).
- [118] Wolfgang K. H. Panofsky and Melba Phillips, *Classical Electricity and Magnetism*, 2nd ed. (Addison-Wesley Publishing Company, Reading, MA, USA, 1962).
- [119] Oleg D. Jefimenko, *Electricity and Magnetism. An introduction to the theory of electric and magnetic fields* (Appleton-Century-Crofts, New York, NY, USA, 1966).
- [120] Mark A. Heald and Jerry B. Marion, *Classical Electromagnetic Radiation*, 3rd ed. (Saunders College Publishing, Fort Worth, TX, USA, 1995).
- [121] B. Thidé, J. Lindberg, H. Then, and F. Tamburini, “Linear and angular momentum of electromagnetic fields generated by an arbitrary distribution of charge and current densities at rest,” (2010), arXiv.org:1001.0954 [physics.class-ph].
- [122] B. Thidé, F. Tamburini, H. Then, C. G. Someda, E. Mari, G. Parisi, F. Spinello, and F. Romanato, “Angular momentum radio,” in *Complex Light and Optical Forces VIII*, Proceedings of SPIE, Vol. 8999, The International Society for Optical Engineering (SPIE, San Francisco, CA, USA, 2014) pp. 89990B–89990B–11.
- [123] There is an error in formula (1) in Thidé *et al.* [122].
- [124] José A. Heras, “Radiation fields of a dipole in arbitrary motion,” *Am. J. Phys.* **62**, 1109–1115 (1994).
- [125] Arthur Stanley Eddington, *The Nature of the Physical World* (Kessinger Publishing, 2010).
- [126] H. Dieter Zeh, *The Physical Basis of The Direction of Time*, 4th ed. (Springer, 2001).
- [127] G. H. Brown, “Turnstile aerials,” *Electronics* **9**, 14–17 (1936).
- [128] Carlo G. Someda, *Electromagnetic Waves*, 2nd ed. (CRC, Boca Raton, FL, USA, 2006).
- [129] H. Shi and M. Bhattacharya, “Mechanical memory for photons with orbital angular momentum,” *J. Phys. B: Atom. Mol. Opt. Phys.* **46**, 151001 (2013).
- [130] H. Shi and M. Bhattacharya, “Coupling a small torsional oscillator to large optical angular momentum,” *J. Mod. Opt.* **60**, 382–386 (2013).
- [131] Markus Aspelmeyer, Tobias J. Kippenberg, and Florian Marquardt, “Cavity optomechanics,” (2013), arXiv.org:1303.0733 [cond-mat, physics:quant-ph].
- [132] T. Bağcı, A. Simonsen, S. Schmid, L. G. Villanueva, E. Zeuthen, J. Appel, J. M. Taylor, A. Sørensen, K. Usami, A. Schliesser, and E. S. Polzik, “Optical detection of radio waves through a nanomechanical transducer,” *Nature* **507**, 81–85 (2014).
- [133] Igor Zutíć, Jaroslav Fabian, and S. Das Sarma, “Spintronics: Fundamentals and applications,” *Rev. Mod. Phys.* **76**, 323–410 (2004).
- [134] Alina M. Deac, Akio Fukushima, Hitoshi Kubota, Hiroki Maehara, Yoshishige Suzuki, Shinji Yuasa, Yoshinori Nagamine, Koji Tsunekawa, David D. Djayaprawira, and Naoki Watanabe, “Bias-driven high-power microwave emission from MgO-based tunnel magnetoresistance devices,” *Nature Phys.* **4**, 803–809 (2008).
- [135] B. Andrei Bernevig, Taylor L. Hughes, and Shou-Cheng Zhang, “Orbitronics: The intrinsic orbital current in p-doped silicon,” *Phys. Rev. Lett.* **95**, 066601 (2005).
- [136] S. S. Verma, “Atomtronics trying to replace Electronics,” *Electronics For You* **43**, 60–64 (2011).
- [137] Yohai Roichman, Bo Sun, Yael Roichman, Jesse Amato-Grill, and David G. Grier, “Optical forces arising from phase gradients,” *Phys. Rev. Lett.* **100**, 013602(4) (2008).
- [138] Gregorius C. G. Berkhout, Martin P. J. Lavery, Johannes Courtial, Marco W. Beijersbergen, and Miles J. Padgett, “Efficient sorting of orbital angular momentum states of light,” *Phys. Rev. Lett.* **105**, 153601(4) (2010).
- [139] Martin P. J. Lavery, David J. Robertson, Anna Sponselli, Johannes Courtial, Nicholas K. Steinhoff, Glenn A. Tyler, Alan E. Willner, and Miles J. Padgett, “Efficient measurement of an optical orbital-angular-momentum spectrum comprising more than 50 states,” *New J. Phys.* **15**, 013024(7) (2013).
- [140] A. Bennis, R. Niemiec, C. Brousseau, K. Mahdjoubi, and O. Emile, “Flat plate for OAM generation in the millimeter band,” in *7th European Conference on Antennas and Propagation (EuCAP)* (2013) pp. 3203–3207.
- [141] Francis E. Low, *Classical Field Theory. Electromagnetism and Gravitation* (John Wiley & Sons, New York, NY, USA, 1997).
- [142] Fabrizio Tamburini, Bo Thidé, Elettra Mari, Giuseppe Parisi, Fabio Spinello, Matteo Oldoni, Roberto A. Ravanelli, Piero Coassini, Carlo G. Someda, and Filippo Romanato, “ N -tupling the capacity of each polarization state in radio links by using electromagnetic vorticity,” (2013), arXiv.org:1307.5569 [physics.optics].
- [143] Juan P. Treviño, Omar López-Cruz, and Sabino Chávez-Cerda, “Segmented vortex telescope and its tolerance to diffraction effects and primary aberrations,” *Opt. Express* **52**, 081605–081605 (2013).
- [144] Michael R. Andrews, Partha P. Mitra, and Robert deCarvalho, “Tripling the capacity of wireless communications using electromagnetic polarization,” *Nature* **409**, 316–318 (2001).
- [145] R. Essiambre and R. W. Tkach, “Capacity trends and limits of optical communication networks,” *Proc. IEEE* **100**, 1035–1055 (2012).
- [146] S. O. Arik, D. Askarov, and J. M. Kahn, “Effect of mode coupling on signal processing complexity in mode-division multiplexing,” *J. Lightw. Technol.* **31**, 423–431 (2013).
- [147] F. Tamburini, B. Thidé, V. Boaga, F. Carraro, M. del Pup, A. Bianchini, C. G. Someda, and F. Romanato, “Experi-

- mental demonstration of free-space information transfer using phase modulated orbital angular momentum radio,” (2013), arXiv.org:1302.2990 [physics.class-ph].
- [148] W. I. Fushchich and A. G. Nikitin, “The complete sets of conservation laws for the electromagnetic field,” *J. Phys. A: Math. Gen.* **25**, L231–L233 (1992).
- [149] T. G. Philbin, “Lipkin’s conservation law, Noether’s theorem, and the relation to optical helicity,” *Phys. Rev. A* **87**, 043843 (2013).
- [150] In certain disciplines a non-standard convention is sometimes used in which the term Lorentz force density denotes only the second term in the RHS of Eqn. (A14b). We follow the standard convention.
- [151] S. J. van Enk and G. Nienhuis, “Commutation rules and eigenvalues of spin and orbital angular momentum of radiation fields,” *J. Mod. Opt.* **41**, 963–977 (1994).
- [152] In fact, the surface integral may also be a vector that is (at most) a function of time t .
- [153] See in particular Section V.5: “Daniel Bernoulli and Euler on the Dependence or Independence of the Law of Moment of Momentum in 1744.”
- [154] Emmy Noether, “Invariante Variationsprobleme,” *Nachr. Ges. Wiss. Göttingen* **1**, 235–257 (1918), English transl.: *Invariant variation problems*, *Transp. Theor. Stat. Phys.*, **1**, 186–207 (1971).
- [155] Dwight E. Neuenschwander, *Emmy Noether’s Wonderful Theorem* (Johns Hopkins University Press, Baltimore, MD, 2011).
- [156] E. Leader, “The angular momentum controversy: What’s it all about and does it matter?” *Phys. Part. Nucl.* **44**, 926–929 (2013).
- [157] Iwo Białynicki-Birula and Zofia Białynicka-Birula, “Canonical separation of angular momentum of light into its orbital and spin parts,” *J. Opt.* **13**, 064014 (2011).
- [158] L. Allen, M. J. Padgett, and M. Babiker, “The orbital angular momentum of light,” in *Prog. Opt.*, Vol. XXXIX, edited by E. Wolf (Elsevier, Amsterdam, Holland, 1999) pp. 291–372.
- [159] Sonja Franke-Arnold, Stephen M. Barnett, Eric Yao, Jonathan Leach, Johannes Courtial, and Miles Padgett, “Uncertainty principle for angular position and angular momentum,” *New J. Phys.* **6**, 1–8 (2004).
- [160] Gabriel Molina-Terriza, Juan P. Torres, and Lluís Torner, “Twisted photons,” *Nature Phys.* **3**, 305–310 (2007).
- [161] Timothy H. Boyer, “Illustrations of the relativistic conservation law for the center of energy,” *Am. J. Phys.* **73**, 953–961 (2005).